GACTTCACCCCTTGATTAA-3′; siRNA-p150b, 5′-CCACCACCAAAGGUUAAGU-3′) (10) or p24 (siRNA-p24, 5′-CCGCATTGCCATACCTGAT-3; siRNA-p24b, 5′-GCUACUUUGCCAGCUAGAG-3′) were transfected at a concentration of 100 nM into HeLa(tc), a HeLa subline (11) or U2OS cells using Oligofectamine (Invitrogen), otherwise indicated in text and figure legends. Dead cells were identified using the trypan blue dye exclusion test. p24 and H2B-GFP were expressed using the pcDNA3 expression vector (Invitrogen).

Rescue Experiments—An siRNA-p24-resistant p24 cDNA was created by changing six nucleotides in the target sequence of siRNA-p24 that have no effect on amino acid sequence (CCGAATAGCAATCCCAGAC; underlined letters indicate replaced nucleotides). Because the target sequence for siRNA-p150 is in the 3′-UTR, we used a p150 cDNA 3′-UTR truncation (a gift of Dr. M. Katsuno and G. Sobue (12)) to generate a siRNA-p150-resistant p150 cDNA. To generate a pantropic retrovirus, HEK 293 cells were co-transfected with three plasmids: pHIT60 expressing murine leukemia virus gag pol (a gift of Dr. A. J. Kingsman (13)), pHCMV-G for vesicular stomatitis virus enveloped pseudotypes (a gift of Dr. T. Friedmann (14)), and pMSCV (Clontech) driving expression of siRNA-resistant p24 or p150 cDNA and IRES-EGFP[2] (15).

Analysis of mRNA and Protein Expression—Real-time quantitative RT-PCR was performed as described previously (16) using primer sets (p24 (forward, 5′-GAGTACATCGACCGCATTGCCATAC-3′ and reverse, 5′-TGATGTGAGCACTGTCCAGCATGG-3′) and p150^{Glued} (forward, 5′-TGCAGGCCACGCTACACCGCTATG-3′ and reverse, 5′-GCAATATCTGTAGCCTCCTGCCCAC-3′)). Immunostaining and image analyses were performed as described (11, 17). Signal specificity was tested by adding antigen for each antibody into the blocking solution. Relative fluorescence intensity was measured using ImageJ software. Immunoprecipitation and immunoblot analyses were performed according to standard procedures (18).

TUNEL—TUNEL assays were performed using the Fluorometric TUNEL assay kit (Promega, Madison, WI). Briefly, cells fixed with paraformaldehyde and ethanol were incubated with fluorescein-dUTP and terminal deoxynucleotidyl transferase for one hour at 37 °C. Cells were propidium iodide-stained immediately prior to flow cytometry analysis (FACSCalibur, BD Biosciences).

Fluorescence in Situ Hybridization (FISH)—HeLa cells cultured on coverglass slips were fixed with 3.7% formaldehyde, denatured on a heat block, and used directly for FISH analysis using a Myc probe complementary to chromosome band 8q24 (Dako, Glostrup, Denmark) according to the manufacturer's protocol.

Reagents—Rabbit anti-p24 polyclonal antibodies were raised against a GST-p24(N) (amino acids 5–36) or a GST-p24(C) polypeptide (amino acids 145–186) and then affinity purified according to standard procedures (18). Commercial antibodies were purchased from the following suppliers: p150^{Glued} from BD Biosciences; actin (product no. 1378 996) from Roche Diagnostics; and α-tubulin (product no. T9026) and γ-tubulin (product no. T6557) from Sigma. Hoechst 33342 was purchased from Invitrogen.

[2] The abbreviations used are: EGFP, enhanced GFP; FISH, fluorescence in situ hybridization; IRES, internal ribosomal entry site.

RESULTS

Down-regulation of p24 and p150^{Glued} Using siRNA—We initially used HeLa(tc) cells, a HeLa subline that allows high efficiency siRNA transfection (typically >90%) (11), for siRNA transfections. HeLa(tc) cells treated with siRNA (100 nM for 24 h) specific for p24 (siRNA-p24) or p150^{Glued} (siRNA-p150) showed a 5-fold approximate decrease in mRNA expression levels relative to cells treated with scrambled control siRNA (control siRNA) (Fig. 1*A*).

We used rabbits to generate two polyclonal antibodies, p24(N) and p24(C), against different portions of p24 (see "Experimental Procedures"). Both antibodies recognized an endogenous p24 protein (Fig. 1*B*, *lane 1*) that migrated to the same position in SDS-polyacrylamide gels as exogenous p24 protein expressed from a eukaryote plasmid expression vector (*lane 4*). As previously reported, the apparent mass of p24 is ~21 kDa, slightly smaller than the mass predicted from the amino acid sequence (4). Cells treated with siRNA-p24 (100 nM) for 48 h expressed 10-fold lower levels of p24 protein relative to untreated cells or cells treated with control siRNA (*lane 3*). Immunoblot analysis using p150^{Glued} antibody revealed a 20-fold reduction in p150^{Glued} protein levels in cells treated with siRNA-p150 for 72 h (Fig. 1*C*).

Similar to previous reports (4), immunostaining of mitotic cells with p24(C) antibody showed p24 localized to kinetochores and centrosomes in prometaphase and metaphase cells with considerable signal remaining in early anaphase (Fig. 1*D*). Although the general localization of p150^{Glued} (Fig. 1*E*) overlaps with p24, some specific differences were distinguished in cells doubly stained with p24 and p150^{Glued} antibodies (Fig. 1*F*). First, staining of mitotic spindles with anti-p150 was strong, whereas only weak fluorescence was detected with anti-p24. Second, although both p24 and p150 signals were detected at prometaphase kinetochores, p150 signal intensity diminished rapidly in metaphase, whereas p24 signals were remained until anaphase. The contrast between the intense p24 immunofluorescence maintained in anaphase centrosomes with diminished p150^{Glued} immunofluorescence that is barely detectable in early anaphase suggests a rapid efflux of p150^{Glued} from centrosomes during metaphase.

When cells were transfected with Cy3-labeled siRNA-p24, the intensity of p24 immunofluorescence in Cy3 staining-positive cells was reduced (Fig. 1*G*, *left panels*). p150^{Glued} signals were also reduced in response to treatment with siRNA-p150 (100 nM) for 72 h (*right panels*).

siRNA-p24 or -p150 Induces Mitotic Disturbances—Although we observed no obvious morphological differences in phase-contrast microscopy images of interphasic HeLa(tc) cells treated for up to 72 h with control siRNA, siRNA-p24, or siRNA-p150 (100 nM) (data not shown), we did observe a significant increase in the mitotic index of cells 48 h after transfection with siRNA-p24 relative to control siRNA (11.1% relative to 4%) ($p < 0.01$, Chi-square test, Fig. 2*A*). In addition,

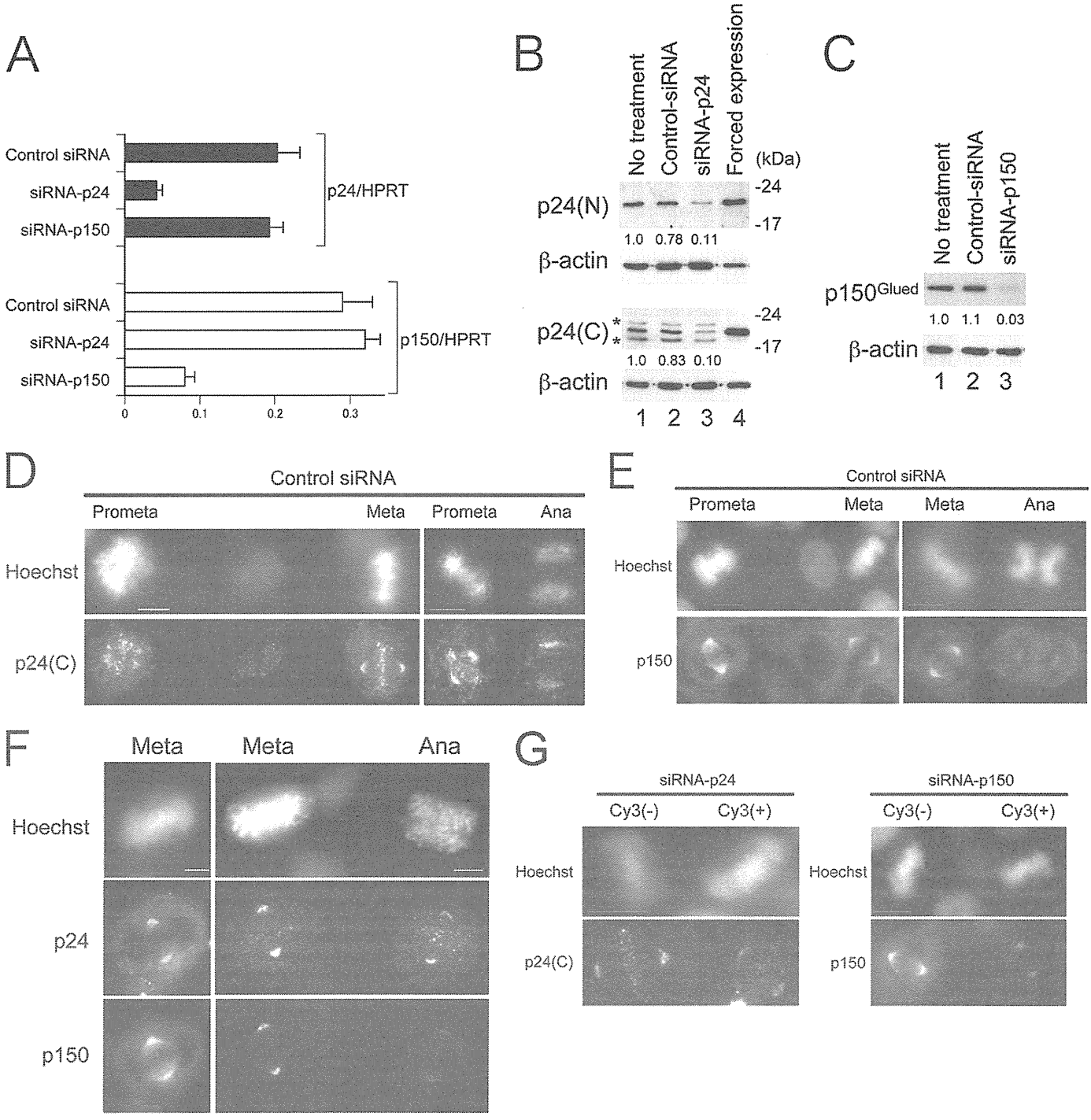

FIGURE 1. **Down-regulation of p24 and p150 by siRNA.** *A*, p24 (*black bars*) and p150^{Glued} (*open bars*) mRNA expression levels in HeLa(tc) cells treated with control siRNA, siRNA-p24, or siRNA-p150 (100 nM) for 24 h. Real-time quantitative PCR data were normalized against hypoxanthine phosphoribosyl transferase (*HPRT*), and the mean and S.D. for three independent experiments is represented. *B*, immunoblot analysis using p24(N), p24(C), or β-actin antibody. *Lane 1*, untreated HeLa(tc) cells; *lane 2*, cells treated with control siRNA (100 nM) for 48 h; *lane 3*, cells treated with siRNA-p24 (100 nM) for 48 h; *lane 4*, HEK 293 cells transfected with pcDNA3-p24, a eukaryotic expression vector. Ratios of relative intensity (p24/actin) measured by densitometry are indicated below each lane. *Asterisks* indicate cross-reactive bands appearing in HeLa but not HEK 293 cells. *C*, immunoblot analysis using p150^{Glued} or β-actin antibody. *Lane 1*, untreated HeLa(tc) cells; *lane 2*, cells treated with control siRNA (100 nM) for 72 h; *lane 3*, cells treated with siRNA-p150 (100 nM) for 72 h. Ratios of relative intensity (p150/actin) measured by densitometry are shown below. *D–G*, immunostaining of mitotic HeLa cells treated with siRNA indicated *above* with antibodies indicated on the *left*. DNA was stained with Hoechst 33342, and the mitotic phase of cells are labeled above. *Bars*, 10 μm (*D*, *E*, and *G*) and 5 μm (*F*). *Meta*, metaphase; *Ana*, anaphase; *Prometa*, prometaphase.

there was also a significant increase ($p < 0.01$) in the number of dead cells (determined by trypan blue dye exclusion) among the cells treated with siRNA-p24 for 48 and 72 h (7.2%, 15/207 and 17.1% 36/211, respectively) and siRNA-p150 for 72 h (8.0%, 16/202) relative to untreated cells (2.0%, 8/401).

Flow cytometric analyses of HeLa cells treated with siRNA-p24 for 48 h and stained with propidium iodide dem-

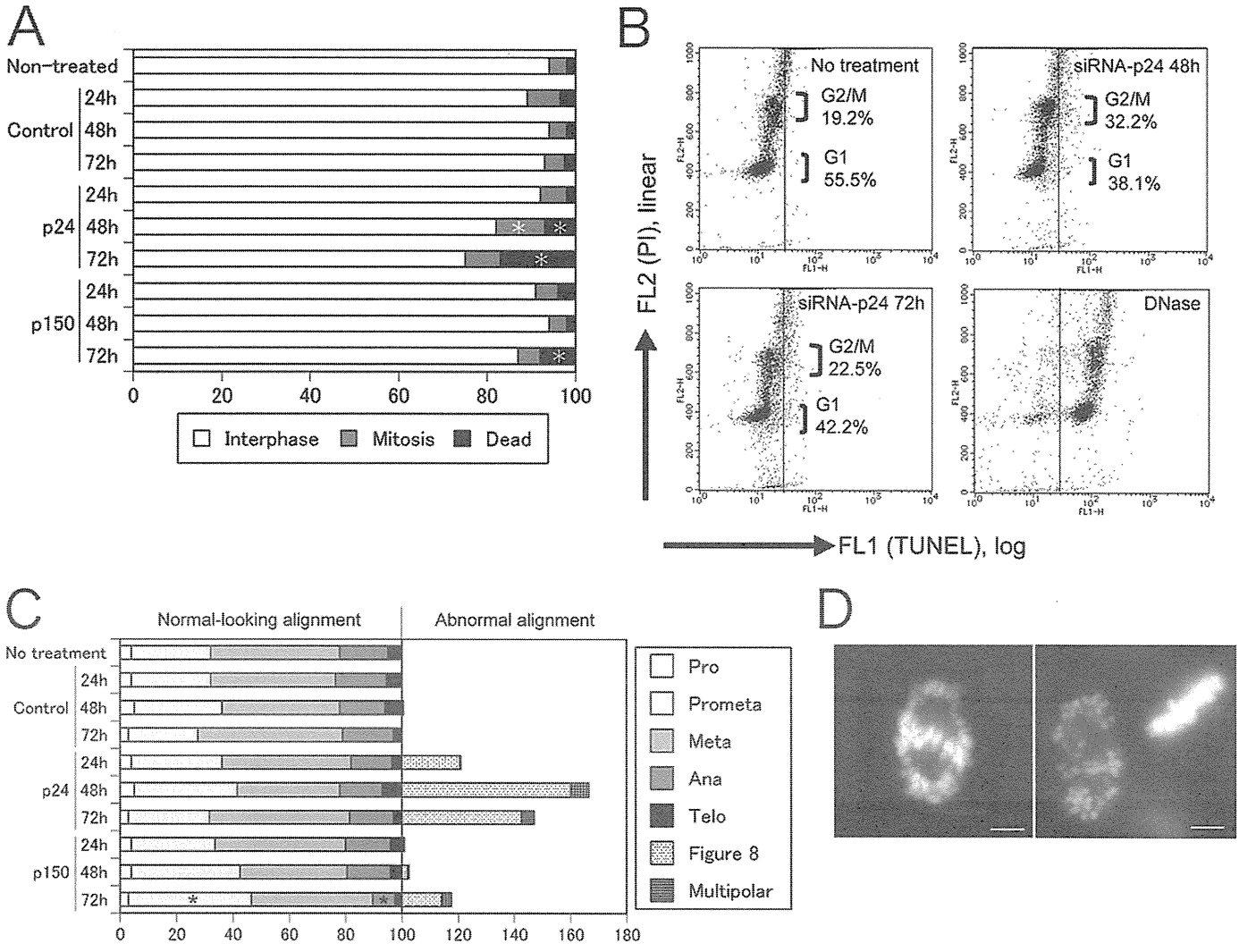

FIGURE 2. **Down-regulation of p24 and p150 induces mitotic abnormalities in HeLa(tc) cells.** *A*, cells were treated with each siRNA for periods indicated on the *left*. From a total of 300 cells counted/treatment, the relative percentages of mitotic, interphase, and dead cells determined by separation of floating cells (mitotic and dead *versus* interphase) and by trypan blue dye exclusion (live *versus* dead) are indicated by *shading*. *Asterisks* indicate a statistically significant ($p < 0.01$) increase relative to the no treatment control using Chi-square test. *B*, cells treated with siRNA-p24 for indicated periods were stained with propidium iodide (*PI*) just prior to flow cytometry and TUNEL analysis. FL1 values on the *horizontal axis* indicate the amount of dUTP polymerized by DNA free 3′ ends, whereas FL2 values on the *vertical axis* show the DNA content. *C*, from a total of 300 cells counted/treatment, the percentages of mitotic cells with normal-looking chromosome alignment (100% total) or abnormal mitosis were determined from observations of Hoechst 33342-stained nuclei. *Asterisks* indicate statistically significant changes in a particular mitotic phase ($p < 0.01$) relative to the no treatment control by Chi-square test. *D*, representative images of Hoescht 33342-stained chromosomes in a figure eight alignment. *Bar*, 5 μm. *Pro*, prophase; *Prometa*, prometaphase; *Meta*, metaphase; *Ana*, anaphase; *Telo*, telophase.

onstrate that siRNA-p24 induces mitotic delay/arrest, in that the G_2/M-phase ratio (Fig. 2*B*, *vertical axis*) was significantly higher in treated cells (32.2%) than in cells without treatment (19.2%) However, the cell death induced by siRNA-p24 does not appear apoptotic because TUNEL assays showed only a small increase in DNA free 3′ ends (Fig. 2*B*, *horizontal axis*; see DNase-treated HeLa cell panel as a positive control) in siRNA-p24-treated cells.

To determine the effects of down-regulation of p24 and $p150^{Glued}$ on mitosis, we analyzed chromosome alignment in Hoechst 33342-stained mitotic cells. Although treatment of cells with control siRNA (100 nM) for up to 72 h did not affect their distribution (Fig. 2*C*), we observed that treatment with siRNA-p24 for 48 h specifically induced one of two distinct patterns of abnormal chromosome alignment in 39.8% (133/334) of mitotic cells (Fig. 2*C*). First, chromosomes in 120 mitotic cells treated with siRNA-p24 for 48 h aligned abnormally to resemble a figure eight pattern (Fig. 2*D*), whereas the same pattern almost never appeared (<1/200) in mitotic cells without siRNA treatment or those treated with control siRNA. Second, 3.9% (13/334) of mitotic cells treated with siRNA-p24 for 48 h demonstrated multipolar mitoses. Among the remaining 201 mitotic cells with normal-looking chromosome alignment, the distribution of cells in each mitotic phase was not altered. Relative to cells treated for 48 h, cells treated with siRNA-p24 for 24 or 72 h showed the same abnormal pattern of chromosome alignment but at a lower frequency (Fig. 2*C*).

In contrast to siRNA-p24-treated cells, cells treated with siRNA-p150 for 48 h showed no significant change in distribution among mitotic phases, and only a few cells demon-

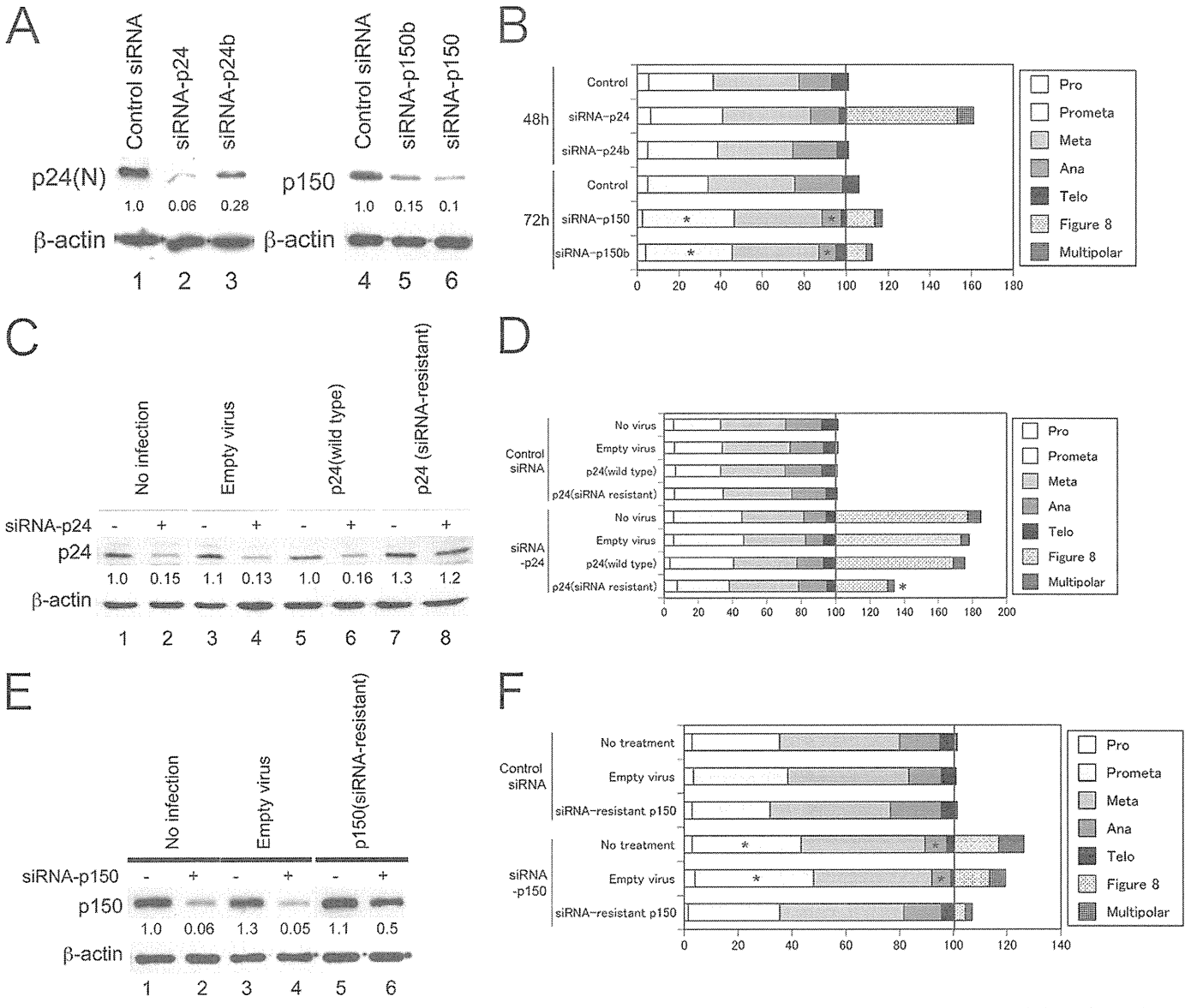

FIGURE 3. *A*, immunoblot analysis using p24(N), p150, or β-actin antibody. HeLa(tc) cells were treated with the siRNA (100 nM) indicated above for 48 (*lanes 1–3*) or 72 h (*lanes 4–6*). Ratios of signal intensity relative to actin (measured using densitometry) are indicated *below each lane*. *B*, *D*, and *F*, the percentages of mitotic cells with normal-looking chromosome alignment (100% total) or abnormal mitosis were determined from observations of Hoechst 33342-stained nuclei in a total of 300 cells/treatment. *Asterisks* indicate statistically significant changes in a particular mitotic phase ($p < 0.01$) relative to the no treatment control using the Chi-square test. *C*, immunoblot analyses using p24(N) or β-actin antibody. *Lanes 1* and *2*, uninfected HeLa(tc) cells; *lanes 3* and *4*, cells infected with empty virus; *lanes 5* and *6*, cells infected with virus containing wild type p24 cDNA; *lanes 7* and *8*, cells infected with virus containing siRNA-resistant p24 cDNA. *Lanes 1*, *3*, *5*, and *7*, cells were treated with control siRNA; *lanes 2*, *4*, *6*, and *8*, cells were treated with siRNA-p24 (100 nM) for 48 h. Ratios of relative signal intensity (p24/actin) are indicated *below each lane*. *E*, immunoblot analysis using p150 or β-actin antibody. *Lanes 1* and *2*, uninfected HeLa(tc) cells; *lanes 3* and *4*, cells infected with empty virus; *lanes 5* and *6*, cells infected with virus containing siRNA-resistant p150 cDNA. *Lanes 1*, *3*, and *5*, cells were treated with control siRNA; *lanes 2*, *4*, and *6*, cells were treated with siRNA-p150 (100 nM) for 72 h. Ratios of relative intensity (p150/actin) are indicated *below each lane*. *Pro*, prophase; *Prometa*, prometaphase; *Meta*, metaphase; *Ana*, anaphase; *Telo*, telophase.

strated the figure eight chromosome alignment seen with siRNA-p24 (Fig. 2*C*). After an additional 24 h of treatment with siRNA-p150, however, we observed a significant increase in the ratio of prometaphase cells and a corresponding decrease in anaphase and telophase cells. In addition, small percentages of mitotic cells showed the figure eight chromosomal alignment (11.9%, 28/236) or multipolar mitoses (3.0%, 7/236).

We also treated cells with secondary siRNAs that target alternative sequences in the p24 or $p150^{Glued}$ genes. When cells were treated with siRNA-p24b, which only reduced p24 levels ~3-fold (Fig. 3*A*), few mitotic cells showed the figure eight chromosome alignment (Fig. 3*B*), suggesting that greater reductions in p24 protein levels are required to induce the figure eight alignment. In contrast, cells treated with siRNA-p150b reduced p150 to levels similar to siRNA-p150 (Fig. 3*A*) and showed similar mitotic disturbances, including an increased ratio of prometaphase cells, a decreased ratio of anaphase/telophase cells, and a few cells with figure eight chromosome alignment.

To exclude the possibility that the figure eight chromosome alignment is an off-target effect of siRNA-p24, we performed

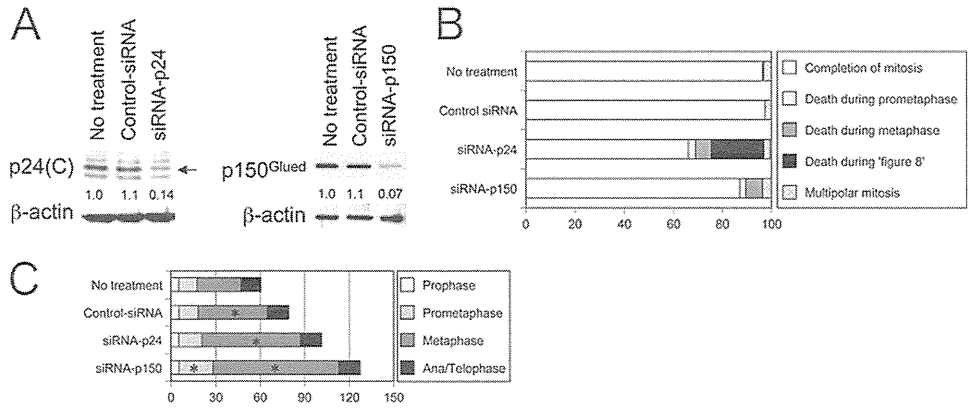

FIGURE 4. **Time-lapse observations of mitotic cells.** *A*, immunoblot analyses of lysates from U2OS cells using p24(C), p150^{Glued}, or β-actin antibody. Cells were treated with the siRNA indicated for 72 h. Ratios of relative intensity (p24 or p150/actin) measured by densitometry are indicated *below each lane*. An *arrow* marks the position of p24. *B*, U2OS cells expressing an H2B-GFP fusion protein were treated with control siRNA or siRNA-p150 for >48 h or with siRNA-p24 for >24 h. Percentages of cells demonstrating termination of mitosis in one of the manners listed on the *right* are indicated with *shading*. *C*, the average duration of each mitotic phase (min) in cells that completed mitosis are indicated by shading. *Asterisks* indicate a statistically significant increase in duration ($p < 0.05$) relative to the no treatment control.

rescue experiments by expressing a siRNA-p24-resistant p24 mRNA from a pantropic retrovirus containing EGFP as a selection marker (see "Experimental Procedures"). EGFP-positive cells were sorted using flow cytometry and then treated with siRNA-p24.

Immunoblot analyses revealed similar levels of p24 in cells infected with retrovirus containing p24 cDNA or siRNA-resistant p24 cDNA (Fig. 3*C*, *lanes 5* and *7*). Following treatment with siRNA-p24 (100 nM for 48 h), uninfected cells, as well as those infected with empty virus or virus containing wild-type cDNA (Fig. 3*C*, *lanes 2*, *4*, and *6*) showed down-regulation of p24 protein. In contrast, there was no significant reduction in p24 levels in cells expressing the siRNA-resistant p24 cDNA (Fig. 3*C*, *lane 8*). Mitotic cells with the figure eight chromosome alignment were observed in cells infected with empty virus (73%) or virus containing wild type cDNA (68.5%) at virtually the same frequency as uninfected cells (77.3%) (Fig. 3*D*). Only cells infected with virus containing the siRNA-resistant cDNA showed a significant reduction in the frequency figure eight mitoses (34.5%, $p < 0.01$), suggesting that p24 is indeed effective in preventing chromosomes from the figure eight alignment.

We also expressed a siRNA-resistant p150 cDNA in HeLa cells using the same pantropic retrovirus system (Fig. 3*E*). Unlike uninfected cells or those infected with the empty virus, cells expressing siRNA-resistant cDNA showed little decrease in p150 levels following siRNA treatment. Similarly, there was no significant increase in prometaphase or decrease in ana/telophase ratios in cells treated with siRNA-p150 (Fig. 3*F*), and the ratio of cells with the figure eight chromosome alignment decreased.

Chromosomes Align into a Figure Eight after Metaphase Arrest—To further analyze the mitotic disturbances induced by p24 or p150^{Glued} down-regulation, we established a U2OS cell line expressing a histone H2B-GFP fusion protein constitutively (19), transfected these cells with control, p24, or p150^{Glued} siRNAs (efficiency typically 70%) and then collected time-lapse images of the transfected cells. In these cells, the magnitude in reduction of p24 or p150^{Glued} protein expression levels by siRNA-p24 or siRNA-p150, respectively, were similar to those achieved in HeLa cells (Fig. 4*A*).

More than 95% of mitotic cells without siRNA treatment or treated with control siRNA completed mitosis (Fig. 4*B*, also see supplemental Movie 1). Cells treated with control siRNA demonstrated a significant elongation of metaphase (46 min in control siRNA-treated cells to compare with 29 min in untreated cells, $p < 0.05$), whereas the durations of prophase, prometaphase, and anaphase and telophase combined (ana/telophase) were not affected (Fig. 4*C*). These data suggest that U2OS cells treated with scrambled siRNA and/or cationic liposome experience a delayed progression through metaphase. Only one of 180 (0.55%) untreated cells and zero of 156 cells treated with control siRNA died while in mitosis.

When cells were treated with siRNA-p24 (100 nM) for >24 h, we observed a significant delay in metaphase (average of 66 min) relative to control siRNA-treated cells (average of 46 min, $p < 0.05$, Fig. 4*C*). There was no elongation in the duration of prometaphase or ana/telophase. We also observed cell death more frequently in siRNA-p24-treated cells: 3% (10/333) or 6.5% (22/333) of mitotic cells underwent cell death during prometaphase or metaphase, respectively (Fig. 4*B*). Intriguingly, in 21.5% (72/333) of siRNA-p24-treated mitotic cells, chromosomes aligned at the metaphase plate during prolonged metaphase broke up into a figure eight pattern (supplemental Movie 2). This similarity to the abnormal chromosome alignment observed in siRNA-p24-treated HeLa cells (Fig. 2*D*) indicates that these are not prometaphase cells but rather post-metaphasic cells that fail to enter anaphase. All 72 cells with figure eight chromosome alignment underwent cell death eventually (an average of 164 min after breakup of chromosome alignment at the metaphase plate) (supplemental Movie 2). Overall, 31% (104/333) of siRNA-p24-treated mitotic cells underwent cell death, whereas these cells in interphase rarely underwent apoptosis (< 0.1%).

In contrast to control siRNA- or siRNA-p24-treated cells, cells treated with siRNA-p150 for >48 h demonstrated delayed prometaphase (average of 23 min to compare with 12 min in control siRNA-treated cells, $p < 0.05$, Fig. 4*C*), during

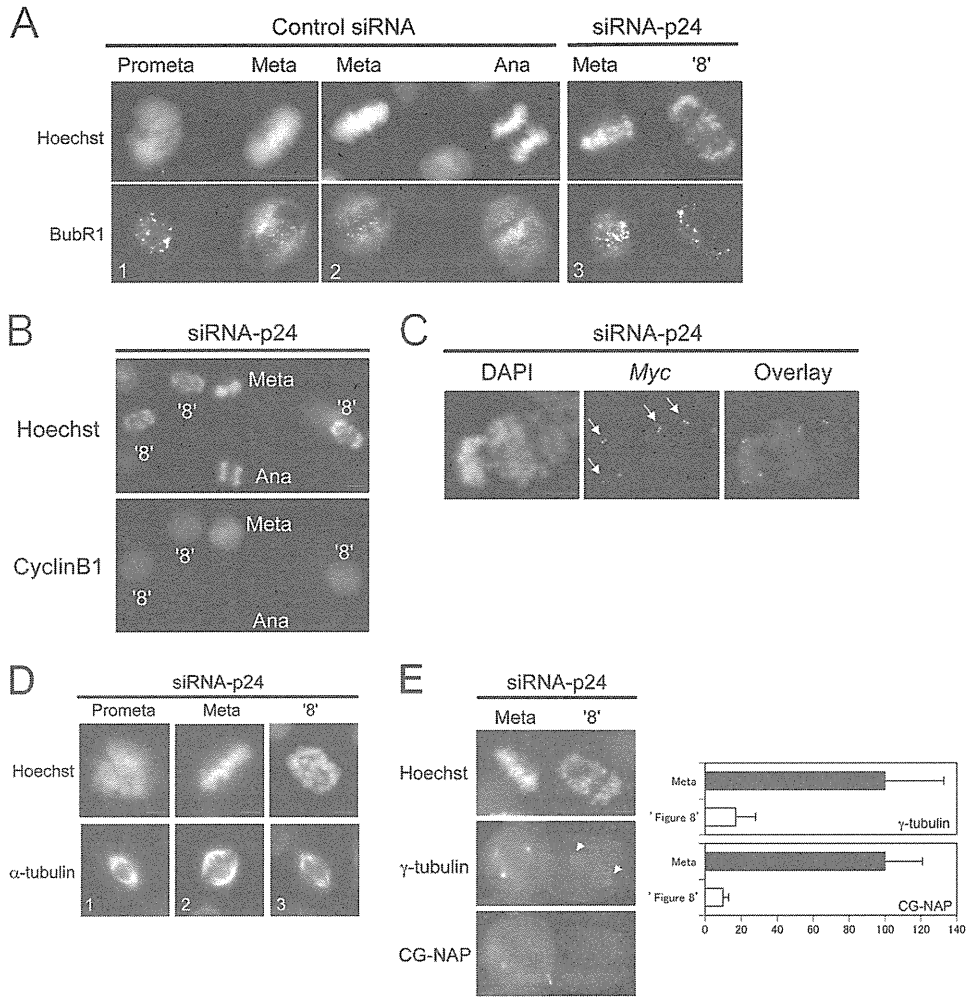

FIGURE 5. **Mechanisms of figure eight chromosome alignment.** *A*, *B*, and *D*, HeLa cells were treated with the siRNA indicated and immunostained with the antibody indicated on the *left*. DNA was stained with Hoechst 33342, and the mitotic phase of cells are labeled *above or within* each image. *Bars*, 10 μm (*A* and *B*) and 5 μm (*D*). *C*, HeLa cells treated with siRNA-p24 were fixed with formaldehyde, denatured, and hybridized with a c-*myc* probe for FISH analysis. DNA was stained with DAPI. *Arrows* mark pairs of dots that indicate sister chromatids. *Bar*, 5 μm. *E*, HeLa cells were treated with siRNA-p24 and immunostained with the antibody indicated on the *left*. Relative fluorescence intensity of proteins in either metaphase (*black bars*) or figure eight (*open bars*) centrosomes (*right panels*). The mean (+ S.D.) intensity of 50 centrosomal areas was measured, and background levels were subtracted. *Bar*, 5 μm. *Prometa*, prometaphase; *Meta*, metaphase; *Ana*, anaphase.

which 2.4% (4/163) underwent cell death. Moreover, the metaphase delay induced by siRNA-p150 (average 85 min, Fig. 4*C*, see Video 3) was more severe than in cells treated with siRNA-p24 and 6.7% (11/163) of siRNA-p150-treated mitotic cells underwent cell death during metaphase. These findings are consistent with previous experiments in which HeLa cells treated with siRNA-p150 showed increased ratios of cells in prometaphase and metaphase relative to cells in anaphase and telophase (Fig. 2*C*). Unlike cells treated with siRNA-p24, none of these mitotic cells showed chromosomes aligned in a figure eight pattern, and all cells that survived through prometaphase and metaphase entered anaphase.

Cells with Figure Eight Chromosome Alignment Share Features with Prometaphase—Our findings demonstrate that down-regulation of either p24 or $p150^{Glued}$ induces severe metaphasic delays. This phenotype is analogous to a previous report about cells that undergo metaphase arrest/delay when dynactin is depleted by dynamitin overexpression (8). In that case, the delay is most likely due to a defect in the function of the dynein-dynactin complex, which removes spindle checkpoint proteins such as BubR1 from kinetochores during metaphase (reviewed in Ref. 20). Indeed, when cells were treated with control siRNA, BubR1 signals localized to kinetochores in prometaphase (Fig. 5*A*, *panel 1*), after which the signal decreased rapidly during metaphase and anaphase (*panels 1* and *2*). In contrast, cells treated with siRNA-p24 showed the same intensity of BubR1 immunofluorescence at the kinetochores of metaphase chromosomes as that in prometaphase cells, including those cells with a figure eight chromosome alignment (*panel 3*).

Despite their similarities in appearance to prometaphase (rather than anaphase) cells, the figure eight chromosome alignment is only seen in cells that have progressed through metaphase (supplemental Movie 2). To further characterize the timing of this unique chromosomal alignment, we looked at expression of cyclin B1, a molecule that is present during metaphase (Fig. 5*B*, *Meta*) and then degraded rapidly in anaphase (*Ana*). We observed positive cyclin B1 immunofluorescence in all mitotic cells with a figure eight chromosome alignment. Moreover, FISH images of the c-*myc* gene on

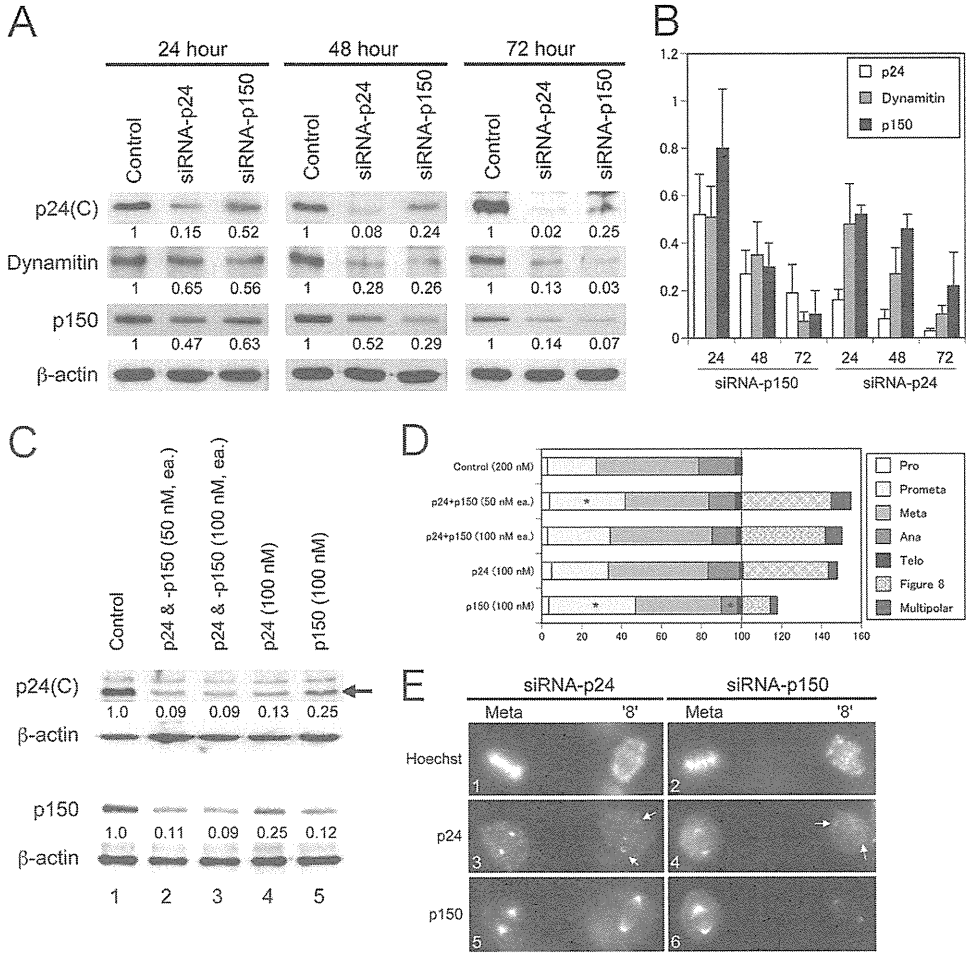

FIGURE 6. **p24 expression levels relate to figure eight configuration.** *A* and *C*, immunoblot analyses using p24(C), dynamitin, p150^{Glued}, or β-actin antibody. HeLa cells were treated with siRNA (100 nM, otherwise indicated) as indicated above for 72 h. Ratios of relative intensity (p24, dynamitin, or p150 actin) measured by densitometry are indicated *below each lane*. Data are representative of four independent experiments that yielded similar results. *B*, average and S.D. protein expression levels in four independent experiments of p24, dynamitin, and p150^{Glued} relative to control siRNA-treated cells. *D*, HeLa (tc) cells were treated with the siRNA indicated on the *left* for 72 h. From a total of 300 cells counted/treatment, the percentages of mitotic cells with normal-looking chromosome alignment (100% total) or abnormal mitosis were determined from observations of Hoechst 33342-stained nuclei. *Asterisks* indicate statistically significant changes in a particular mitotic phase ($p < 0.01$) relative to the no treatment control using a Chi-square test. *E*, HeLa cells were treated with the siRNA indicated above and immunostained with the antibody indicated on the *left*. DNA was stained with Hoechst 33342, and the mitotic phase of each cell is labeled *above*. *Bar*, 10 μm. *Pro*, prophase; *Prometa*, prometaphase; *Meta*, metaphase; *Ana*, anaphase; *Telo*, telophase. '8', figure eight.

chromosome band 8q24 indicate that sister chromatids in cells with figure eight alignment have yet to segregate because four pairs of dots are visible on chromosomes in figure eight cells (Fig. 5*C*, *arrows*; FISH with chromosome 8-specific centromeric probes revealed that HeLa(tc) cells have four chromosome 8 (data not shown)). These data suggest that cells with figure eight chromosome alignment are most like prometaphase cells.

Because the alignment of chromosomes on the metaphase plate is mediated by tension between the spindle poles, reversal of the mitotic process by siRNA-p24 interference may be due to reductions in spindle tension. Using α-tubulin immunostaining, we compared the density and morphology of spindles in cells at different stages of mitosis. In cells displaying a figure eight configuration (Fig. 5*D*, *panel 3*), the robust fluorescence characteristic of metaphase mitotic spindles (*panel 2*) reverted to a shape and intensity more characteristic of mitotic spindles in prometaphase (*panel 1*). Moreover, the marked decrease in immunostaining signal intensity for γ-tubulin and CG-NAP (pivotal components of the γ-tubulin ring complex that provides microtubule nucleation sites) in figure eight-stage cells relative to metaphase cells (Fig. 5*E*) suggests that p24 is required to maintain the integrity of metaphase centrosomes.

p24 Levels Relate to Figure Eight Chromosome Alignment—In parallel experiments conducted in two different cell lines (HeLa or U2OS), metaphase arrest/delay was induced similarly following treatment with either siRNA-p24 or siRNA-p150; however, siRNA-p24 was significantly more effective than siRNA-p150 in inducing the figure eight chromosome alignment during metaphase (Figs. 2*C* and 4, *B* and *C*). We did not observe any change in expression of p150^{Glued} and p24 mRNAs following treatment with siRNA-p24 or siRNA-p150, respectively (Fig. 1*A*). However, both of these siRNAs did reduce protein expression levels of p24, p150^{Glued}, and dynamitin in HeLa(tc) cells (Fig. 6*A*). Similar results were obtained in U2OS cells (data not shown). Similar to previous reports demonstrating that overexpression of dynamitin disrupts dynactin structure (2), our results with p24 and p150^{Glued} suggest that balanced availability of all

components is required to maintain the stability of the dynactin complex.

To test whether changes in p24 expression levels are sufficient to induce the figure eight chromosome alignment, we treated cells with siRNAs and then measured the expression levels of dynactin components and observed alterations in chromosome alignment. When cells were treated with siRNA-p150 for 24 or 48 h, expression levels of p24, dynamitin, and p150^{Glued} relative to control cells were ~25% or higher (Fig. 6*B*), but no mitotic abnormalities were observed (Fig. 2, *A* and *C*). Treatment with siRNA-p150 for 72 h reduced the expression levels of dynamitin and p150^{Glued} to <10% and p24 to ~20%, and this treatment induced metaphase arrest/delay and a few cells with the figure eight chromosome alignment (Fig. 2*C*). In contrast, treatment of cells with siRNA-p24 for 24 or 48 h reduced the expression levels of p24 to less than 15%, while maintaining relatively high (>25%) levels of dynamitin and p150^{Glued}. In this case, more mitotic cells showed a figure eight chromosome alignment (Fig. 2*C*).

We also treated HeLa(tc) cells with a combination of both siRNA-p24 and siRNA-p150 (50 or 100 nM each) for 72 h. Although this procedure reduced both p24 and p150 expression levels to ~10% of those in control cells (Fig. 6*C*, *lanes 2* and *3*), the ratio of cells in the figure eight alignment (42–45%) was virtually the same as cells treated with siRNA-p24 alone (43%, Fig. 6*D*), in which p24 and p150 expression are reduced to ~10 and 25% of control cells, respectively (Fig. 6*C*, *lane 4*). Once again, cells treated with siRNA-p150 alone that expressed p24 at 25% and p150 at 10% of control cells (*lane 5*) showed only a small number (~10%) of mitotic cells with the figure eight configuration (Fig. 6*D*). These data demonstrate that among all components of the dynactin complex, manipulation of p24 expression levels is most likely to result in cells assuming the figure eight configuration.

Further evidence in support of this correlation was observed when treated cells were immunostained simultaneously for p24 and p150^{Glued}. p24 immunofluorescence at centrosomes of mitotic HeLa(tc) cells treated with siRNA-p24 was markedly less intense in cells with the figure eight chromosome alignment relative to metaphasic cells in the same microscopic field (Fig. 6*E*, *panel 3*). Intriguingly, p150 immunofluorescence at centrosomes in most (23/25) of these figure eight cells was as bright as the signal in metaphasic cells (Fig. 6*E*, *panel 5*). In contrast, in cells treated with siRNA-p150, both p24 and p150 immunofluorescence signals in figure eight cells were markedly reduced (Fig. 6*E*, *panels 4* and *6*) in all cells observed (25/25). These results suggest that failure of p24 to accumulate in mitotic centrosomes induces figure eight chromosome alignment.

DISCUSSION

In this report, we treated HeLa and U2OS cells with siRNAs specific for p24 or p150^{Glued}, two components of the projecting arm of the dynactin complex. Time-lapse observations reveal that treatment of siRNA-p24 induces severe metaphase delay. In >40% of metaphase cells struggling to enter anaphase, chromosomes aligned on the metaphase plate break away and assume a configuration resembling a figure eight. In time, all cells with the figure eight alignment die without completing mitosis. In contrast with p24, cells treated with siRNA-p150 demonstrate severe delays in metaphase, but most cells do not assume the figure eight alignment and ultimately progress to anaphase. Neither p24 nor p150^{Glued} appears to be involved in the progression of anaphase and telophase.

Reductions in p24 or p150^{Glued} protein levels induce metaphase arrest/delay (Fig. 4*C* and supplemental Movies 1–3). This is consistent with a previous report in which cells overexpress dynamitin, which down-regulates dynactin function, also undergo metaphase arrest/delay (8). Failure to remove spindle checkpoint proteins such as BubR1 from kinetochores (Fig. 5*A*) results in metaphase delay because checkpoint proteins inhibit cdc20, a specific activator of the anaphase-promoting complex/cyclosome (reviewed in Ref. 20). Because anaphase-promoting complex/cyclosome functions as an E3 ubiquitin ligase, mitotic checkpoint proteins that are remain on kinetochores delay ubiquitin-dependent degradation of cyclin B1 (Fig. 5*B*) or securin, which then inhibits cohesin hydrolysis and blocks chromosome segregation (Fig. 5*C*).

Nonetheless, the transition of chromosomes from a metaphase to a figure eight configuration does not appear to be a direct result of spindle checkpoint protein retention at kinetochores. Because there is a marked reduction of γ-tubulin and CG-NAP signals at mitotic centrosomes in cells with the figure eight chromosome alignment (Fig. 5*E*), insufficient amounts of γ-TuRC in metaphase centrosomes appear to be one of the major factors driving the phenotype. Thus, we hypothesize that loss of spindle microtubule tension (Fig. 5*D*) is the defect that induces chromosomes to break away from alignment at the metaphase plate.

The two functions of the dynactin complex are to remove spindle checkpoint proteins from kinetochores and to maintain centrosome integrity until entry into anaphase. Although we have observed that neither of these functions are disturbed when expression levels of p24, dynamitin, or p150^{Glued} remain at least 25% of control levels (siRNA-p150 for 48 h, see Figs. 2*C* and 6*A*), we did note that a 10-fold reduction in the expression of either p24 or p150^{Glued} impaired the removal of checkpoint proteins, resulting in metaphase delay. In contrast, chromosome integrity and the resulting formation of figure eight cells was only induced with a 10-fold reduction in p24 levels but not with a reduction in p150^{Glued}. Immunofluorescence experiments also emphasized a correlation between accumulation of p24 (but not p150^{Glued}) in centrosomes and figure eight chromosome alignment (Fig. 6*E*). These data suggest that p24 acts independently of p150^{Glued} in metaphase centrosomes, where it helps maintain chromosome integrity and prevents breakaway until entry into anaphase.

Although it is generally accepted that p24, dynamitin, and p150^{Glued} function together in the dynactin projecting arm (2), we and others (4, 21) have observed that the localization of different dynactin components during mitosis varies considerably. For example, p24 immunofluorescence is strong at centrosomes relative to mitotic spindles or kinetochores. This is particularly evident during early anaphase (Fig. 1, *E* and *F*)

when p150^{Glued} immunofluorescence is barely detectable. In conclusion, our results suggest that p24 operates independently from the dynactin complex in binding to metaphase centrosomes and maintaining their integrity. To explore this hypothesis further, we are currently investigating the function of p24 in metaphase centrosomes in greater detail.

Acknowledgments—We thank Dr. K. Kevin Pfister (University of Virginia) for kindly providing antibodies against p24, Dr. M. Katsuno and G. Sobue (Nagoya University) for providing expression vectors for p150^{Glued}, and M. Nakamura for excellent technical assistance.

REFERENCES

1. Musacchio, A., and Salmon, E. D. (2007) *Nat. Rev. Mol. Cell Biol.* **8,** 379–393
2. Schroer, T. A. (2004) *Annu. Rev. Cell Dev. Biol.* **20,** 759–779
3. Pfister, K. K., Benashski, S. E., Dillman, J. F., 3rd, Patel-King, R. S., and King, S. M. (1998) *Cell Motil Cytoskeleton* **41,** 154–167
4. Karki, S., LaMonte, B., and Holzbaur, E. L. (1998) *J. Cell Biol.* **142,** 1023–1034
5. Eckley, D. M., and Schroer, T. A. (2003) *Mol. Biol. Cell* **14,** 2645–2654
6. Amaro, I. A., Costanzo, M., Boone, C., and Huffaker, T. C. (2008) *Genetics* **178,** 703–709
7. Burkhardt, J. K., Echeverri, C. J., Nilsson, T., and Vallee, R. B. (1997) *J. Cell Biol.* **139,** 469–484
8. Whyte, J., Bader, J. R., Tauhata, S. B., Raycroft, M., Hornick, J., Pfister, K. K., Lane, W. S., Chan, G. K., Hinchcliffe, E. H., Vaughan, P. S., and Vaughan, K. T. (2008) *J. Cell Biol.* **183,** 819–834
9. Cheung, P. Y., Zhang, Y., Long, J., Lin, S., Zhang, M., Jiang, Y., and Wu, Z. (2004) *J. Biol. Chem.* **279,** 45308–45311
10. Dixit, R., Levy, J. R., Tokito, M., Ligon, L. A., and Holzbaur, E. L. (2008) *J. Biol. Chem.* **283,** 33611–33619
11. Oshimori, N., Ohsugi, M., and Yamamoto, T. (2006) *Nat. Cell Biol.* **8,** 1095–1101
12. Katsuno, M., Adachi, H., Minamiyama, M., Waza, M., Tokui, K., Banno, H., Suzuki, K., Onoda, Y., Tanaka, F., Doyu, M., and Sobue, G. (2006) *J. Neurosci.* **26,** 12106–12117
13. Soneoka, Y., Cannon, P. M., Ramsdale, E. E., Griffiths, J. C., Romano, G., Kingsman, S. M., and Kingsman, A. J. (1995) *Nucleic Acids Res.* **23,** 628–633
14. Burns, J. C., Friedmann, T., Driever, W., Burrascano, M., and Yee, J. K. (1993) *Proc. Natl. Acad. Sci. U.S.A.* **90,** 8033–8037
15. Kuribara, R., Kinoshita, T., Miyajima, A., Shinjyo, T., Yoshihara, T., Inukai, T., Ozawa, K., Look, A. T., and Inaba, T. (1999) *Mol. Cell. Biol.* **19,** 2754–2762
16. Kuribara, R., Honda, H., Matsui, H., Shinjyo, T., Inukai, T., Sugita, K., Nakazawa, S., Hirai, H., Ozawa, K., and Inaba, T. (2004) *Mol. Cell. Biol.* **24,** 6172–6183
17. Tokai-Nishizumi, N., Ohsugi, M., Suzuki, E., and Yamamoto, T. (2005) *Mol. Biol. Cell* **16,** 5455–5463
18. Shinjyo, T., Kuribara, R., Inukai, T., Hosoi, H., Kinoshita, T., Miyajima, A., Houghton, P. J., Look, A. T., Ozawa, K., and Inaba, T. (2001) *Mol. Cell. Biol.* **21,** 854–864
19. Shi, Q., and King, R. W. (2005) *Nature* **437,** 1038–1042
20. Lu, Y., Wang, Z., Ge, L., Chen, N., and Liu, H. (2009) *Cell Struct. Funct.* **34,** 31–45
21. Echeverri, C. J., Paschal, B. M., Vaughan, K. T., and Vallee, R. B. (1996) *J. Cell Biol.* **132,** 617–633

Aberrant induction of LMO2 by the E2A-HLF chimeric transcription factor and its implication in leukemogenesis of B-precursor ALL with t(17;19)

Kinuko Hirose,[1] Takeshi Inukai,[1] Jiro Kikuchi,[2] Yusuke Furukawa,[2] Tomokatsu Ikawa,[3] Hiroshi Kawamoto,[3] S. Helen Oram,[4] Berthold Göttgens,[4] Nobutaka Kiyokawa,[5] Yoshitaka Miyagawa,[5] Hajime Okita,[5] Koshi Akahane,[1] Xiaochun Zhang,[1] Itaru Kuroda,[1] Hiroko Honna,[1] Keiko Kagami,[1] Kumiko Goi,[1] Hidemitsu Kurosawa,[6] A. Thomas Look,[7] Hirotaka Matsui,[8] Toshiya Inaba,[8] and Kanji Sugita[1]

[1]Pediatrics, School of Medicine, University of Yamanashi, Yamanashi, Japan; [2]Stem Cell Regulation, Center for Molecular Medicine, Jichi Medical School, Tochigi, Japan; [3]Laboratory for Lymphocyte Development, RIKEN Research Center for Allergy and Immunology, Yokohama, Japan; [4]Department of Haematology, Cambridge Institute for Medical Research, Cambridge University, Cambridge, United Kingdom; [5]Developmental Biology, National Research Institute for Child Health and Development, Tokyo, Japan; [6]Department of Pediatrics, Dokkyo Medical School, Tochigi, Japan; [7]Pediatric Oncology, Dana-Farber Cancer Institute, Boston, MA; and [8]Molecular Oncology, Research Institute for Radiation Biology and Medicine, Hiroshima University, Hiroshima, Japan

LMO2, a critical transcription regulator of hematopoiesis, is involved in human T-cell leukemia. The binding site of proline and acidic amino acid–rich protein (PAR) transcription factors in the promoter of the *LMO2* gene plays a central role in hematopoietic-specific expression. E2A-HLF fusion derived from t(17;19) in B-precursor acute lymphoblastic leukemia (ALL) has the transactivation domain of E2A and the basic region/leucine zipper domain of HLF, which is a PAR transcription factor, raising the possibility that E2A-HLF aberrantly induces LMO2 expression. We here demonstrate that cell lines and a primary sample of t(17;19)-ALL expressed LMO2 at significantly higher levels than other B-precursor ALLs did. Transfection of *E2A-HLF* into a non-t(17;19) B-precursor ALL cell line induced *LMO2* gene expression that was dependent on the DNA-binding and transactivation activities of E2A-HLF. The PAR site in the *LMO2* gene promoter was critical for E2A-HLF-induced LMO2 expression. Gene silencing of *LMO2* in a t(17;19)-ALL cell line by short hairpin RNA induced apoptotic cell death. These observations indicated that E2A-HLF promotes cell survival of t(17;19)-ALL cells by aberrantly up-regulating LMO2 expression. LMO2 could be a target for a new therapeutic modality for extremely chemo-resistant t(17;19)-ALL. (*Blood*. 2010;116(6):962-970)

Introduction

Transcription factors that regulate normal hematopoiesis are frequently involved in leukemogenesis[1,2] through 2 types of chromosomal translocation: one causes in-frame fusion of 2 genes and the resultant chimeric transcription factor acquires novel functions and/or functionally disrupts the normal gene products, and the other causes aberrant activation of a transcription factor gene due to juxtaposition to a strong enhancer of the immunoglobulin or T-cell receptor (TCR) loci. The *LMO2* gene, located on the short arm of chromosome 11 at band 13 (11p13), was discovered from a recurrent site of translocations in T-cell acute lymphoblastic leukemia (T-ALL) as a paradigm of the latter type of translocation.[3,4] LMO2 is a member of the LIM-only zinc finger protein family and is present in a transcription factor complex[5] that also includes E2A, TAL1, GATA1, and LDB1 in erythroid cells.[6] Within this complex, LMO2 mediates the protein-protein interactions by recruiting LDB1,[7] whereas TAL1, GATA1, and E2A directly bind to the specific DNA target sites.[6,8] Homozygous null mutation of *Lmo2* showed embryonic lethality due to lack of yolk sac erythropoiesis,[9] and chimeric animals produced from homozygous-deficient embryonic stem cells demonstrated a requirement of *Lmo2* in adult hematopoiesis[10] and angiogenic remodeling of the vasculature.[11] *Lmo2* is expressed in long-term repopulating hematopoietic stem cells[12] and in hematopoietic progenitors,[9] and its expression is maintained in erythroid cells during differentiation. In contrast, *Lmo2* expression is repressed in terminally differentiated granulocytes, macrophages, T cells, and B cells[9] with the exception of germinal center B cells.[13-15] During T-cell development, *Lmo2* is expressed in immature CD4/CD8 double-negative thymocytes and is down-regulated as maturation progresses,[16] and transgenic mice expressing *Lmo2* using a thymocyte-specific promoter developed an accumulation of CD4/CD8 double-negative thymocytes and eventually a T-cell lymphoma.[17-20] Of note, among X-linked severe combined immunodeficiency patients receiving retroviral *IL2Rγc* gene therapy, 2 patients developed T-ALL due to aberrant activation of *LMO2* via integration of the retroviral vector in the *LMO2* gene.[16,21,22] These observations suggested that deregulated *LMO2* increases susceptibility to T-cell malignancies by blocking differentiation. Although similar down-regulation of LMO2 was suggested during B-cell development,[9] the significance of LMO2 expression in B-precursor ALL remains totally unclarified.

The *LMO2* gene has 2 transcriptional promoters and comprises 6 exons, of which exons 4, 5, and 6 encode the protein.[23] The distal and proximal promoters are located upstream of exon 1 or 3 of the larger transcripts, respectively, and the 2 resultant transcripts encode the same open reading frame. The proximal promoter is active in hematopoietic progenitor and endothelial cells, dependent

Submitted September 21, 2009; accepted April 15, 2010. Prepublished online as *Blood* First Edition paper, June 2, 2010; DOI 10.1182/blood-2009-09-244673.

The online version of this article contains a data supplement.

The publication costs of this article were defrayed in part by page charge payment. Therefore, and solely to indicate this fact, this article is hereby marked "advertisement" in accordance with 18 USC section 1734.

on activation of 3 conserved Ets sites,[24] but transgenic analysis demonstrated that the proximal promoter alone is insufficient for full expression of the *Lmo2* gene in hematopoietic cells.[24] The distal promoter is involved in hematopoietic-specific *LMO2* gene expression that is dependent on activation of the proline and acidic amino acid-rich protein (PAR) site in the *LMO2* gene promoter.[25] The PAR transcription factors belong to the basic region/leucine zipper (bZIP) factor family and include hepatic leukemic factor (HLF),[26,27] albumin gene promoter D-site binding protein (DBP),[28] and thyrotroph embryonic factor (TEF).[29] Among the PAR transcription factors, it has been demonstrated that TEF shows the highest potential to activate the *LMO2* promoter in erythroid cells.[25]

t(17;19)(q21-q22;p13) is a relatively rare translocation among childhood ALL cases[2] and is linked with the B-precursor phenotype. E2A-HLF derived from t(17;19) promotes anchorage-independent growth of murine fibroblasts[30,31] and protects cells from apoptosis induced by growth factor deprivation,[32-34] and *E2A-HLF* transgenic mice develop T-cell malignancies.[35,36] In E2A-HLF chimera, the transactivation domain of E2A fuses to the bZIP dimerization and DNA-binding domain of HLF, one of the PAR transcription factors.[26,27] As a result, E2A-HLF recognizes the consensus sequence of PAR transcription factors as a dimer and transactivates downstream target genes.[27,31,37,38] Considering the critical involvement of the PAR site in the distal promoter of the *LMO2* gene in the hematopoietic-specific expression of *LMO2*,[25] E2A-HLF might induce aberrant expression of *LMO2* through the distal promoter. In the present study, we show aberrantly higher expression of LMO2 in t(17;19)-ALL as one of the direct targets of E2A-HLF. The biologic significance of LMO2 in leukemogenesis of t(17;19)-ALL is also investigated and discussed.

Methods

Leukemia cell lines and patient sample

Four ALL cell lines with 17;19 translocation (UOC-B1, HALO1, YCUB2, Endo-kun) were used in this study. As B-precursor ALL cell lines, 9 *MLL*-rearranged ALL cell lines (KOPN-1, KOPB-26, KOCL-33, -44, -45, -50, -51, -58, and -69),[39] 6 Philadelphia chromosome (Ph1)–positive ALL cell lines (KOPN-30bi, -57bi, -66bi, -72bi, YAMN-73, and -91),[40] 7 t(1;19)-ALL cell lines (697, KOPN-34, -36, -60, -63, YAMN-90, and -92), and 6 other ALL cell lines including 1 with t(12;21) (Reh) and 5 with others (KOPN-35, -61, -62, -79, and -84) were used. Seven T-ALL cell lines (KOPT-K1, -5, -6, -11, YAMT-12, Jurkat, and MOLT4F), 4 Burkitt B-cell lines (KOBK-130, Daudi, Namalwa, and Raji), and 4 Epstein-Barr virus (EBV)–transformed normal B-cell lines (YAMB-1, -3, -4, and -9) were also used. All cell lines were maintained in RPMI1640 medium supplemented with 10% fetal calf serum (FCS) in a humidified atmosphere of 5% CO_2 at 37°C. Analysis of a sample from a patient with t(17;19)-ALL was approved by the Ethical Review Board of the University of Yamanashi. Mononuclear cells (blasts > 95%) that had been isolated from bone marrow aspirates of the patient by Ficoll-Hypaque density centrifugation were stored in liquid nitrogen with 15% dimethyl sulfoxide in fetal calf serum (FCS).

Isolation of normal B precursors

The $CD34^+$ population was separated from human cord blood mononuclear cells (MNCs) using MACS MicroBeads (Miltenyi Biotec) and, subsequently, $CD34^+/CD19^-$ and $CD34^+/CD19^+$ populations were sorted by flow cytometry (FACS Vantage; Becton Dickinson) using FITC-Lineage marker (CD3, CD4, CD8, CD11b, CD56, CD235a, CD41a) in combination with PE-CD34 and APC-CD19. $CD19^+/IgM^-$ and $CD19^+/IgM^+$ populations were sorted from human cord blood MNCs by flow cytometry using FITC-Lineage marker in combination with PE-IgM and APC-CD19. The $CD19^+$ population was also directly separated from peripheral blood MNCs with MACS MicroBeads. RNA was extracted from each population using RNeasy mini kit (QIAGEN), and cDNA was synthesized using SuperScript VILO cDNA synthesis kit (Invitrogen).

Western blot analysis

Cells were solubilized in Nonidet P-40 lysis buffer, and total cellular proteins were separated by sodium dodecyl sulfate–polyacrylamide gel electrophoresis (SDS-PAGE) under reducing conditions. After transfer onto nitrocellulose membrane and blocking with 5% nonfat dry milk in 0.05% Tween-20 Tris [tris(hydroxymethyl)aminomethane]–buffered saline (TBS), the membrane was incubated with the primary antibodies in 5% milk in TBS. Goat anti–human LMO2 and mouse anti–human α-Tubulin antibodies were purchased from R&D Systems and Sigma-Aldrich, respectively. Rabbit anti–human antibodies against E2A and HLF(C) were established as previously reported.[37] Membranes were incubated with horseradish peroxidase–conjugated rabbit anti–goat, goat anti–mouse, and goat anti–rabbit IgG (1:1000 dilution; MBL) and were then developed using the enhanced chemiluminescence kit (Amersham Pharmacia Biotech).

Real-time PCR analysis

Total RNA was extracted using Trizol reagent (Invitrogen). Reverse transcription (RT) was performed using random hexamer (Amersham Bioscience) by Superscript II reverse transcriptase (Invitrogen), and then the cDNA product was incubated with RNase (Invitrogen). For quantitative real-time polymerase chain reaction (PCR) of *LMO2*, triplicated samples containing cDNA with Taqman Universal PCR Master Mix (Applied Biosystems) and Gene Expression Product (exons 1/2, HS00951959_m1; exons 4/5, HS00277106_m1; Applied Biosystems) were amplified according to the manufacturer's protocol using KOPT-6 derived from T-ALL with t(11;14) as a control. As an internal control for relative gene expression, quantitative real-time PCR for *GAPDH* (Hs 99999905_m1, Applied Biosystems) was performed.

Semiquantitative PCR of transcripts derived from distal and proximal promoters

RNA transcripts originating from the distal *LMO2* promoter were quantified with forward primer 5′-CAAAGCAGGCAATTAGCCC-3′ and reverse primer 5′-CCTCTCCACTAGCTACTGC-3′, which are situated in exons 1 and 2, respectively. Total *LMO2* expression was quantified with forward primer 5′- GAGCTGCGACCTCTGTGG-3′ and reverse primer 5′-CACCCGCATTGTCATCTCAT-3′, which are situated in exons 5 and 6, respectively. Standard curves were created against a single copy of the *LMO2* full-length cDNA subcloned into the pGEMT Easy (Promega) backbone. The assay was performed in triplicate, and the mean quantity of proximal promoter-derived transcripts was directly calculated by subtracting the mean quantity of distal promoter-derived transcripts from the mean quantity of total transcripts. To consider the degree of approximation of the calculated mean, the following equation was considered: $\mathrm{var}(a+b) = \mathrm{var}(a)+\mathrm{var}(b)+2\mathrm{cov}(a,b)$. The standard deviation of the quantity of proximal promoter-derived transcripts is therefore assumed to be represented as follows: SD prox LMO2 = sqrt [(SD total LMO2)^2- (SD distal LMO2)^2].

Construction of eukaryotic expression vectors and transfection

Expression plasmids containing wild-type and mutated *E2A-HLF* cDNA were constructed with the pMT-$CB6^+$ eukaryotic expression vector (a gift from F. Rauscher III, Wistar Institute, Philadelphia, PA),[32] which contains the inserted cDNA under control of a sheep metallothionein promoter. ΔAD1/ΔLH mutant and Basic region mutant (BX) were prepared as previously reported.[30,33] Transfectants were generated by electroporation followed by selection using neomycin analog G418 as previously reported.[33]

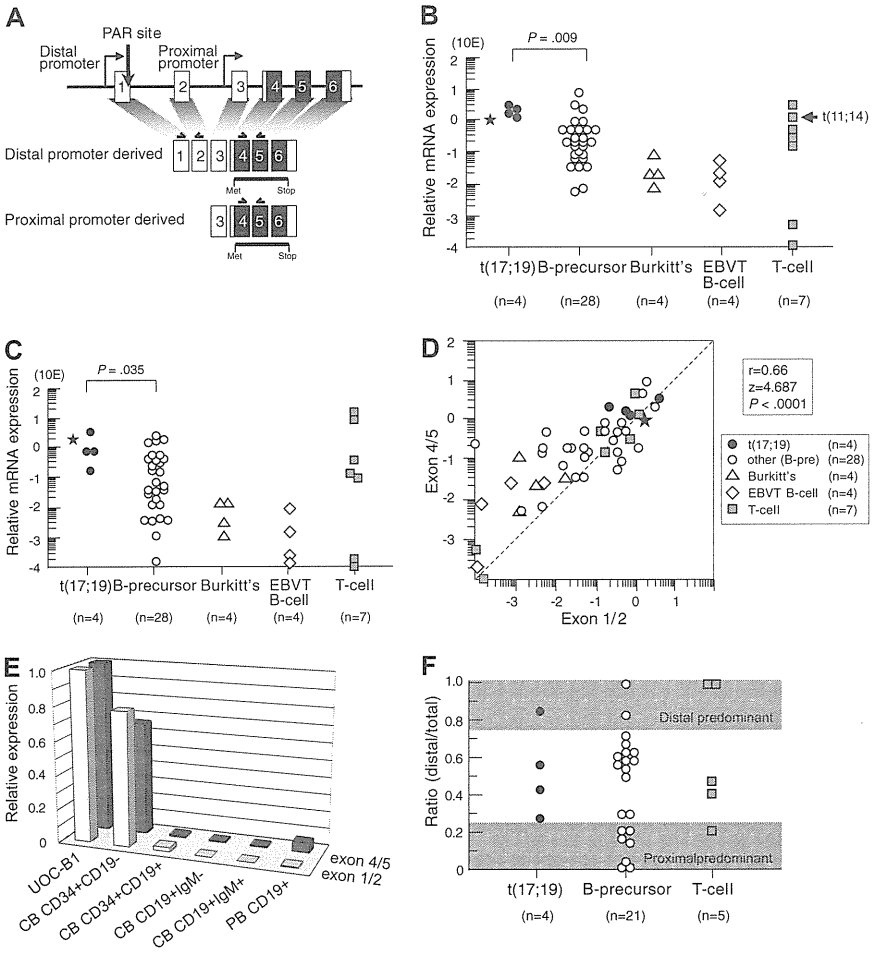

Figure 1. LMO2 gene expression in t(17;19)-ALL. (A) Schematic representation of 2 *LMO2* gene promoters and primers for real-time RT-PCR analysis. Primers directed toward exons 1 and 2 specifically detect transcripts derived from the distal promoter, and those directed toward exons 4 and 5 detect transcripts derived from both the distal and proximal promoters. (B) Relative *LMO2* gene expression determined by real-time RT-PCR using the primers for exons 4 and 5. Arrow indicates T-ALL cell line with t(11;14), and asterisk indicates the level of *LMO2* transcripts in a primary leukemia sample from the patient with t(17;19)-ALL. The *P* value determined by Mann-Whitney test is indicated. (C) Relative *LMO2* gene expression determined by real-time RT-PCR using the primers for exons 1 and 2. (D) Correlation between the levels of *LMO2* transcripts quantified by the primers for exons 4 and 5 (vertical axis) and those for exons 1 and 2 (horizontal axis). (E) *LMO2* gene expression in $CD34^+/CD19^-$, $CD34^+/CD19^+$, $CD19^+/IgM^-$, and $CD19^+/IgM^+$ populations of cord blood mononuclear cells (MNCs) and $CD19^+$ population of peripheral blood MNCs. Relative *LMO2* gene expression was determined by real-time RT-PCR using UOC-B1 as a control with the primers for exons 1 and 2 and the primers for exons 4 and 5. The gene expression level of *β-actin* was used as an internal control. SE of triplicated samples was always less than 10%. (F) Ratio of *LMO2* gene expression derived from the distal promoter to total *LMO2* gene expression in ALL cell lines. *LMO2* gene expression in the cell lines that expressed a total *LMO2* gene level of at least 10 times lower than that in UOC-B1 was semiquantifiedby real-time PCR with the specific primers for *LMO2* transcripts sourced at the distal promoter and for total *LMO2* transcripts. The dark areas indicate a proximal promoter-predominant pattern (ratio < 0.25) or a distal promoter-predominant pattern (ratio > 0.75).

Electrophoretic mobility shift assay

Nuclear extracts of cells were prepared and binding reactions were performed as previously reported.[31,37] Briefly, a ^{32}P-end-labeled oligonucleotide probe containing wild-type HLF consensus sequence (CS; 5′-GCTACAT*ATTACGTAAT*AAGCGTT-3′) was incubated in 10 μL of binding buffer and 5 μL of nuclear lysates in the presence of 1 μg of shared calf thymus DNA. In the competition inhibition experiments, an approximately 100-fold molar excess of the unlabeled oligonucleotide was added to the reaction mixture. Polyvalent HLF(C) or E2A rabbit antiserum was added to the nuclear lysates before the DNA-binding reaction.

Reporter assays

−512/+428 *Kpn*I-*Hin*dIII fragment and −512/+249 *Kpn*I/*Bgl*II fragment of the *LMO2* gene generated by PCR were cloned into the pGL3 basic vector (Promega). −512/+428 PAR^M that has the sequence *CATCGAT*-CAT instead of ATTACATCAT in the PAR site was generated by PCR mutagenesis. All constructs were subjected to nucleotide sequence analysis to verify the appropriate insertions. pGL3 control vector and pRL-TK vector were used as the positive control and internal control of transfection efficiency, respectively. For transfection, wild type and E2A-HLF-expressing Nalm6 cells were plated at 5×10^5 cells/well in a 24-well plate and a total of 5 μg of luciferase reporter plasmid, 1 μg of pRL-TK and 2 μL of lipofectamine (Invitrogen) in 50 μL of serum-free medium (Opti-MEM I; Invirogen) were added. After 24 hours of culture, 100μM $ZnSO_4$ at final concentration was added to induce E2A-HLF expression. Cells were harvested 48 hours after transfection and lysed in 50 μL of lysis buffer (Promega). Activities of firefly and *Renilla* luciferases in each lysate were measured sequentially using the Dual-Luciferase reporter assay system from Promega by a luminometer according to the manufacturer's instructions.

Lentivirus shRNA/siRNA expression vectors and infection

pLL3.7 lentiviral vector was engineered to produce short hairpin RNAs (shRNAs) under the control of mouse U6 promoter and co-express green fluorescent protein (GFP) as a reporter gene by cytomegalovirus-derived promoter–GFP expression cassette.[41] Short interfering RNA (siRNA) target sequences were designed to be homologous to the wild-type *LMO2* cDNA sequence, and oligonucleotides were subcloned into pLL3.7.[42] The selected sequences were submitted to BLAST search to assure that only *LMO2* was targeted. Among 5 sets of oligonucleotides containing siRNA target sequences, the following set was selected for further analysis due to the specificity and efficiency: 5′-Tgacgcatttcggttgagaa*TTCAAGAGA*Att-ctcaaccgaaatgcgtcTTTTTTC-3′(Blunt-siRNA/sense hairpin-siRNA/anti-sense-polyA-*Xho*I/forward);5′-TCGAGAAAAAAgacgcatttcggttgagaa-TCTCTTGAAttctcaaccgaaatgcgtcA-3′(reverse). The control vector contained the following as ineffective set: 5′-Tgcaatattacatatacgcc*TTCAA-GAGA*ggcgtatatgtaatattgcTTTTTTC-3′ (forward); 5′-TCGAGAAA-AAAgcaatattacatatacgccTCTCTTGAAggcgtatatgtaatattgcA-3′(reverse). pLL3.7 shRNA vector or control vector was cotransfected with packaging vector into 293FT cells and the resulting supernatant was collected after 36 hours.[42] Lentivirus was recovered after ultracentrifugation and infected to UOC-B1 cells.

Results

Aberrant expression of LMO2 in t(17;19)-ALL

We first analyzed *LMO2* gene expression in 4 t(17;19)-ALL cell lines, UOC-B1, HALO1, YCUB2, and Endo-kun, by real-time RT-PCR using 2 different sets of primers (Figure 1A): one set

directed toward exons 1 and 2 that is specific for the transcripts derived from the distal promoter, and the other set directed toward exons 4 and 5 that is specific for the transcripts derived from both the distal and proximal promoters. Real-time RT-PCR analysis using the primers specific for exons 4 and 5 demonstrated that all 4 t(17;19)-ALL cell lines expressed *LMO2* transcripts at an equivalent level to that in KOPT6, a T-ALL cell line that aberrantly expresses LMO2 as a result of t(11;14) (Figure 1B). The level of *LMO2* transcripts in t(17;19)-ALL cell lines was significantly higher than that in 28 other B-precursor ALL cell lines ($P = .009$, Mann-Whitney test) including Ph1-ALL, t(1;19)-ALL, and *MLL*+ALL (supplemental Figure 1A, available on the *Blood* Web site; see the Supplemental Materials link at the top of the online article). Real-time RT-PCR analysis using the primers specific for exons 1 and 2 demonstrated that the level of *LMO2* transcripts derived from the distal promoter in t(17;19)-ALL cell lines was also significantly higher than that in the other B-precursor ALL cell lines (Figure 1C and supplemental Figure 1B). A strong correlation was observed between the levels of *LMO2* transcripts quantified by the 2 sets of primers among the 47 cell lines ($r = 0.66$, $P < .0001$; Figure 1D). The primary sample from a t(17;19)-ALL patient also demonstrated high levels of *LMO2* transcripts (Figure 1B-C). Consistent with down-regulation of *LMO2* gene expression during the progression of normal B-cell development,[9] the gene expression level of *LMO2* in Burkitt B-cell lines as well as EBV-transformed normal B-cell lines was unanimously low. Thus, the *LMO2* gene expression level during B-cell development was analyzed using fractions of cord blood and peripheral blood MNCs (Figure 1E). The *LMO2* gene expression level in the $CD34^+/CD19^-$ population of cord blood MNCs was almost equivalent to that in UOC-B1, and it was markedly down-regulated in the $CD34^+/CD19^+$ population. This low expression level was sustained in the $CD19^+/IgM^-$ and the $CD19^+/IgM^+$ populations of cord blood MNCs as well as in the $CD19^+$ population of peripheral blood MNCs.

Next, the contribution of the distal promoter was analyzed in those cell lines that expressed the total *LMO2* gene at a level of at least 10 times lower than that in UOC-B1 by real-time PCR using standard curves, which were created against DNA template of the full-length *LMO2* cDNA that was subcloned into the vector as a single copy. The ratio of the quantity of *LMO2* transcripts sourced at the distal promoter to the quantity of total *LMO2* transcripts in the t(17;19)-ALL cell lines was 0.26 to 0.83 (Figure 1F), indicating that both the distal and the proximal promoters contributed to *LMO2* gene expression. None of the 4 t(17;19)-ALL cell lines showed a proximal promoter-predominant pattern (ratio < 0.25), while 7 of 21 other B-precursor ALL cell lines and 1 of 5 T-ALL cell lines showed a proximal promoter-predominant pattern.

We next analyzed LMO2 protein expression by Western blotting using α-tubulin expression as an internal control. Consistent with the gene expression level, LMO2 protein was aberrantly expressed in all 4 t(17;19)-ALL cell lines at a similarly high level to that in the T-ALL cell line with t(11;14) (Figure 2A). compared with other B-precursor ALL cell lines (Figure 2B), the t(17;19)-ALL cell lines expressed significantly higher levels of LMO2 protein ($P = .005$, Mann-Whitney test). Consistent with the low gene expression level, protein expression of LMO2 was undetectable in both Burkitt B-cell lines and EBV-transformed normal B-cell lines. Strong correlations were observed between the levels of LMO2 protein and *LMO2* transcripts analyzed by the primers specific for exons 4 and 5 ($r = 0.72$, $P < .0001$, Figure 2C) and those for exons 1 and 2 ($r = 0.42$, $P = .0089$). These observations indicated that t(17;19)-ALL cells aberrantly express LMO2.

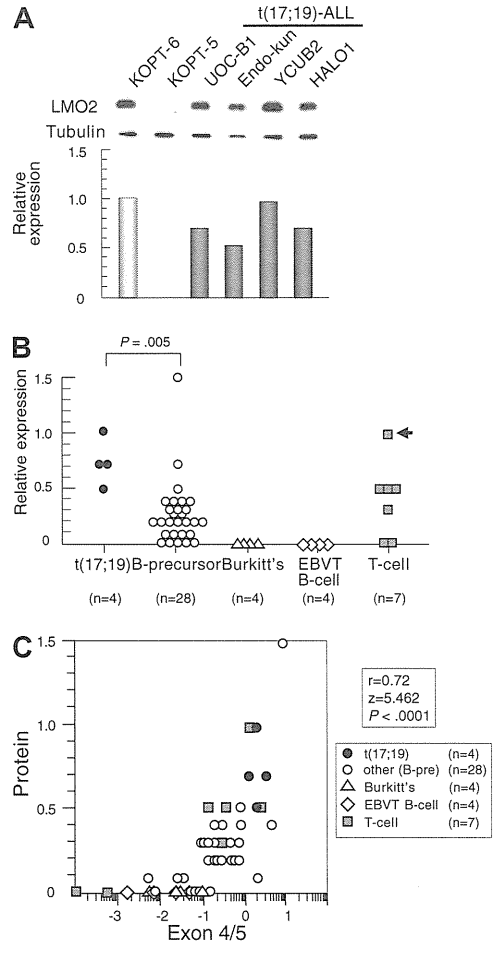

Figure 2. LMO2 protein expression in t(17;19)-ALL. (A) Western blot analysis of LMO2. Relative expression of each cell line was determined by quantifying the intensity of each band using KOPT6, a T-ALL cell line with t(11;14), as a positive control and KOPT-5, a T-ALL cell line without LMO2 expression, as a negative control, and normalized by the level of α-tubulin expression as an internal control. (B) Relative level of LMO2 protein expression. The *P* value determined by Mann-Whitney test is indicated. (C) Correlation between levels of relative protein expression of LMO2 (vertical axis) and gene expression of *LMO2* analyzed by real-time RT-PCR using the primers for exons 4 and 5 (horizontal axis).

Up-regulation of the *LMO2* gene expression by E2A-HLF

To test the possibility that aberrant expression of *LMO2* in t(17;19)-ALL cells is driven by E2A-HLF, we transfected *E2A-HLF* into B-precursor ALL cell line 697, which has t(1;19) and expresses approximately 100-fold lower level of *LMO2* gene than the t(17;19)-ALL cell lines, using a zinc-inducible vector. In E2A-HLF-transfected 697 cells, E2A-HLF was up-regulated to a level equivalent to that in UOC-B1 cells within 4 hours of the addition of zinc to the culture medium (Figure 3A). When analyzed by real-time RT-PCR using primers specific for exons 4 and 5 (Figure 3B), *LMO2* gene expression was up-regulated by the addition of zinc in the E2A-HLF-transfected 697 cells but not in the wild-type 697 cells. When the *LMO2* gene expression derived from the distal and the proximal promoters was differentially semiquantified by real-time PCR (Figure 3C), significant gene expression derived from the distal promoter was immediately induced within 4 hours after the addition of zinc. Subsequently, significant gene expression derived from the proximal promoter was induced within

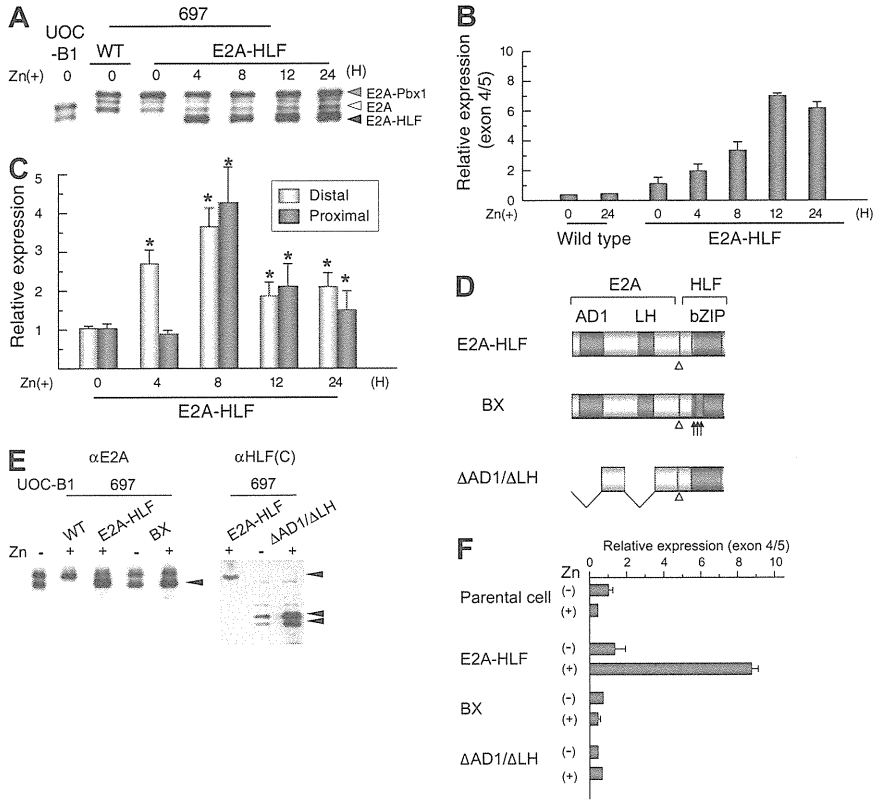

Figure 3. Induction of *LMO2* gene expression by E2A-HLF. (A) Induction of E2A-HLF expression. Lysates of wild type (WT) and a clone of *E2A-HLF*–transfected 697 cells as well as UOC-B1 cells harvested at the indicated time after the addition of zinc were blotted with an anti-E2A serum. Gray, white, and black arrowheads indicate E2A-Pbx1, E2A, and E2A-HLF, respectively. (B) Time course analysis of *LOM2* gene expression after induction of E2A-HLF. Levels of *LMO2* transcripts were quantified by real-time RT-PCR using the primers for exons 4 and 5, normalized by *GAPDH* gene expression as an internal control. Changes in fold induction of *LMO2* gene expression level to that in wild type 697 cells cultured in the absence of zinc are shown as the mean ± SE of triplicate samples. (C) Time course analysis of *LOM2* gene expression derived from the distal and proximal promoters after induction of E2A-HLF. Levels of *LMO2* transcripts in E2A-HLF–transfected 697 cells cultured in the presence of zinc were semiquantified by real-time RT-PCR with the specific primers for *LMO2* transcripts sourced at the distal promoter and for total *LMO2* transcripts. Changes in fold induction of *LMO2* gene expression level to that in E2A-HLF–transfected cells cultured in the absence of zinc are shown as the mean ± SE of triplicate samples. Asterisks indicate the significant gene induction determined by t-test. (D) Schematic diagram of mutants of E2A-HLF. (E) Western blot analysis of mutants of E2A-HLF. Lysates of UOC-B1 cells and wild-type (WT) and clones of 697 cells transfected with *E2A-HLF*, *BX*, and *ΔAD1/ΔLH* cultured in the absence or presence of zinc for 24 hours were blotted with E2A (left panel) and HLF(C) (right panel) antisera. (F) *LMO2* gene expression in mutant *E2A-HLF*–transfected 697 cells. Wild-type (WT) and transfectants of 697 cells were cultured in the absence or presence of zinc for 24 hours, and the levels of *LMO2* transcripts were quantified by real-time RT-PCR. Changes in fold induction of *LMO2* gene expression level to that in wild-type 697 cells cultured in the absence of zinc are shown as the mean ± SE of triplicate samples.

8 hours after the addition of zinc. These observations suggest that the distal and the proximal promoters of the *LMO2* gene sequentially contribute to E2A-HLF–induced *LMO2* gene expression. We further tested 2 types of E2A-HLF mutants in 697 cells. BX contains substitutions of 6 critical basic amino acids in the basic region of HLF to abolish DNA-binding ability, while ΔAD1/ΔLH lacks 2 transactivation domains of E2A to abolish transactivation ability but retain DNA-binding ability (Figure 3D).[30,33] Despite almost equivalent levels of expression of each mutant protein to that of E2A-HLF (Figure 3E), the gene expression level of *LMO2* remained unchanged after the addition of zinc (Figure 3F), indicating that both the DNA-binding and transactivation abilities of E2A-HLF are required for induction of *LMO2* gene expression.

Essential role of the PAR site in the distal promoter of the *LMO2* gene for up-regulation of *LMO2* expression by E2A-HLF

To determine whether E2A-HLF binds to the PAR site in the distal promoter of the *LMO2* gene, we performed electrophoretic mobility shift assay using HLF-CS sequence as a probe in the presence of the double-stranded oligomers listed in Figure 4A as competitors.[25] The DNA-protein complex of E2A-HLF, which was ablated or supershifted in the presence of anti-HLF(C) (Figure 4B lane 1) or anti-E2A (Figure 4B lane 2) antisera, respectively, was competed by the addition of oligomers centered on the PAR site in the distal promoter region (Figure 4B lanes 7-9), although less effectively than unlabeled HLF-CS probe (Figure 4B lanes 3-6). The oligomers containing 2-bp replacement in the 3′ region immediately outside of the PAR site (PAR^{TG}) effectively competed the formation of DNA-protein complex (Figure 4B lane 11), while those containing 2-bp (PAR^{CA}) or 4-bp (PAR^{M}) replacement within the PAR site (Figure 4B lanes 10,12) did not, indicating that the PAR site in the distal promoter of the *LMO2* gene is critical for the binding of E2A-HLF. We also performed electrophoretic mobility shift assay using the sequence of the PAR site in the distal promoter of the *LMO2* gene as a probe, but could not find significant binding (data not shown). High levels of sequence conservation among the mammalian sequences were reported across the entire *LMO2* genomic region.[24] The PAR site sequence in the distal promoter is highly conserved in chimpanzee (*Pan troglodytes*), cow (*Bos Taurus*), and mouse (*Mus musculus*; supplemental Figure 2A), suggesting that the PAR site plays an essential role in the *LMO2* gene expression in these mammalian species. Consistent with conservation of the PAR site in the distal promoter of mouse *lom2* gene, when *E2A-HLF* was transfected into FL5.12 cells, an IL-3–dependent mouse pro-B cell line, using zinc inducible vector as reported before,[33] *lmo2* gene expression derived from the distal

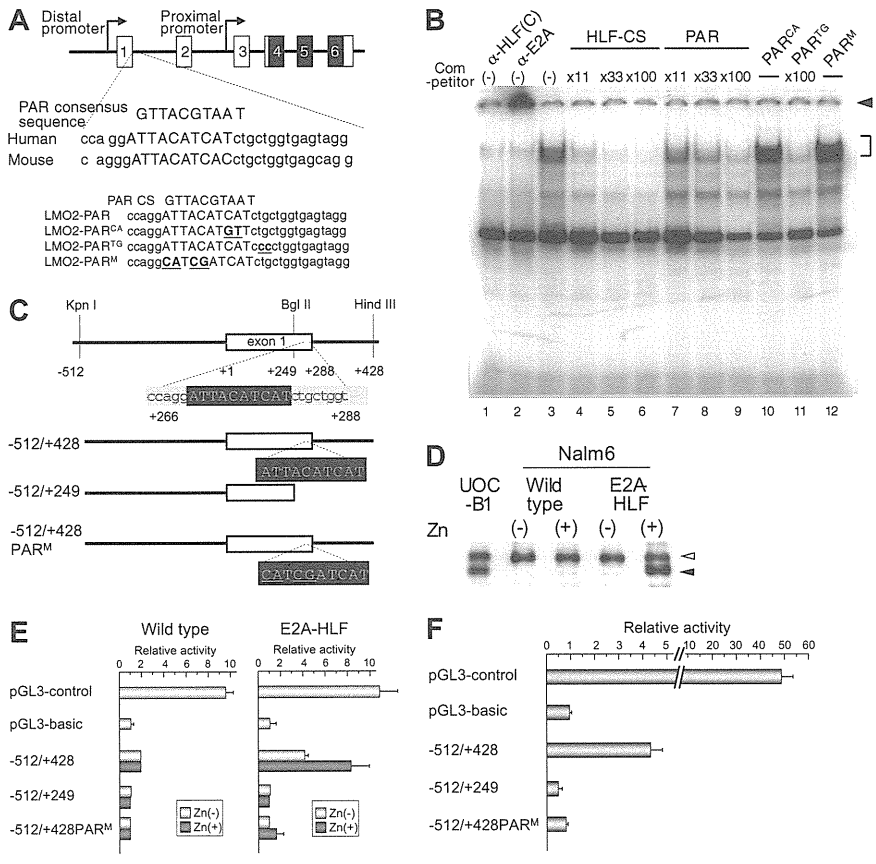

Figure 4. Involvement of the PAR site in the distal promoter of *LMO2* gene in E2A-HLF–induced LMO2 expression. (A) Schematic representation of the proline and acidic amino acid–rich protein (PAR) site in the distal promoter of the *LMO2* gene and oligonucleotides used as competitors in electrophoretic mobility shift assay. Mutations in the sequence are underlined. (B) Electrophoretic mobility shift assay performed in nuclear extracts from UOC-B1 cells using an HLF-CS sequence as a probe in the presence of a series of double-stranded oligomers as competitors (lanes 4-12) or anti-HLF(C) (lane 1) and anti-E2A (lane 2) sera. The molar ratio of cold competitor to probe is indicated in each lane. The specific DNA-protein complex is indicated by the bracket and the supershifted complex is indicated by the arrowhead. (C) Schematic representation of 3 reporter constructs for reporter assay. Mutations in the sequence are underlined. (D) Western blot analysis of E2A-HLF–transfected Nalm6 cells. Lysates of UOC-B1 cells and wild type and *E2A-HLF* transfected-Nalm6 cells cultured in the absence or presence of zinc for 24 hours were blotted with E2A antisera. Open and closed arrowheads indicate E2A and E2A-HLF, respectively. (E) Luciferase assay in E2A-HLF–transfected Nalm6 cells. Assays were performed in wild type and E2A-HLF–transfected Nalm6 cells cultured in the absence or presence of zinc for 24 hours after transient transfection of each reporter plasmid. The values were normalized for transfection efficiencies using a cotransfected *Renilla* luciferase construct. (F) Luciferase assay in YCUB2 cells. The values were normalized for transfection efficiencies using a cotransfected *Renilla* luciferase construct.

promoter was up-regulated by the addition of zinc in the *E2A-HLF*-transfected FL5.12 cells but not in the empty vector–transfected FL5.12 cells (supplemental Figure 2B).

We next performed luciferase assay of 3 reporter constructs[25] (Figure 4C) in Nalm6 cells transfected with *E2A-HLF* using a zinc-inducible vector. In E2A-HLF-transfected Nalm6 cells, E2A-HLF was faintly expressed in the absence of zinc, and it was up-regulated in the presence of zinc to a level equivalent to that in UOC-B1 cells (Figure 4D). When the −512/+428 reporter construct was transiently transfected, transcriptional activity was up-regulated in E2A-HLF–transfected Nalm6 cells in the presence of zinc whereas it was virtually silent in the wild-type Nalm6 cells (Figure 4E). Transcriptional activity of the distal promoter was completely abolished by deletion or mutation of the PAR site. Exactly the same pattern of promoter activities was verified in YCUB2, one of the t(17;19)-ALL cell lines (Figure 4F), demonstrating that E2A-HLF up-regulates *LMO2* gene expression by binding to the PAR site in the distal promoter of the *LMO2* gene.

Induction of apoptosis by shRNA for *LMO2* in a t(17;19)-ALL cell line

To study the significance of aberrant *LMO2* expression in leukemogenesis in t(17;19)-ALL, we introduced shRNA against *LMO2* into the t(17;19)-positive UOC-B1 cell line using a lentivirus vector, which contains *GFP* cDNA for cell sorting (Figure 5A).[41] The expression level of the *LMO2* gene in the GFP-positive (+) population of shRNA virus–infected UOC-B1 (shRNA/UOC-B1) cells was approximately 1000-fold lower than that in the GFP+ control virus–infected UOC-B1 (control/UOC-B1) cells when analyzed by real-time RT-PCR using the primers for exons 4 and 5 (Figure 5B). Despite infection with the same multiplicity of infection, the percentage of the GFP+ population decreased in the shRNA/UOC-B1 cells, in particular the GFP^{high} population that is supposed to express a higher level of shRNA, whereas it was unchanged in the control/UOC-B1 cells (Figure 5C). The percentage of the GFP+ population in shRNA/UOC-B1 cells was significantly lower than that in the control/UOC-B1 cells (Figure 5D, 7.5% vs 30.5% on day 5 after infection; $P = .003$ by t test). By contrast, when infected into 697 cells, a t(1;19)-ALL cell line used as a control, the percentage of the GFP+ population was stable in both the shRNA-virus-infected and the control virus-infected cells (Figure 5C).

To determine whether the reduction in the GFP+ cells in shRNA/UOC-B1 cells was due to cell death or cell-cycle arrest, we performed flow cytometric analysis of BrdU/7-AAD double staining on day 3 after infection (Figure 5E). The percentage of sub-G0/G1 apoptotic cells in the GFP+ shRNA/UOC-B1 cells was significantly higher than that in the control/UOC-B1 cells (12.4% vs 3.6%; $P = .014$ by t test, Figure 5F), while the percentages of cells in the G0/G1, S, and G2/M phases were almost unchanged. Moreover, as shown in Figure 5G, the percentage of caspase-3–activated cells in the GFP+ shRNA/UOC-B1 cells was significantly higher than that in the control/UOC-B1 cells (21.4% vs 0.5%; $P = .00087$ by t test). These observations demonstrate that induction of apoptotic cell death is responsible for the reduction in the GFP+ population among shRNA/UOC-B1 cells.

Discussion

In T-ALL, 2 mechanisms of aberrant expression of the *LMO2* gene have been well characterized: one is translocation of the *LMO2* gene, leading to its combination with enhancers or other regulatory elements of *TCR* genes,[1,3,4,43] and the other is cryptic deletion at

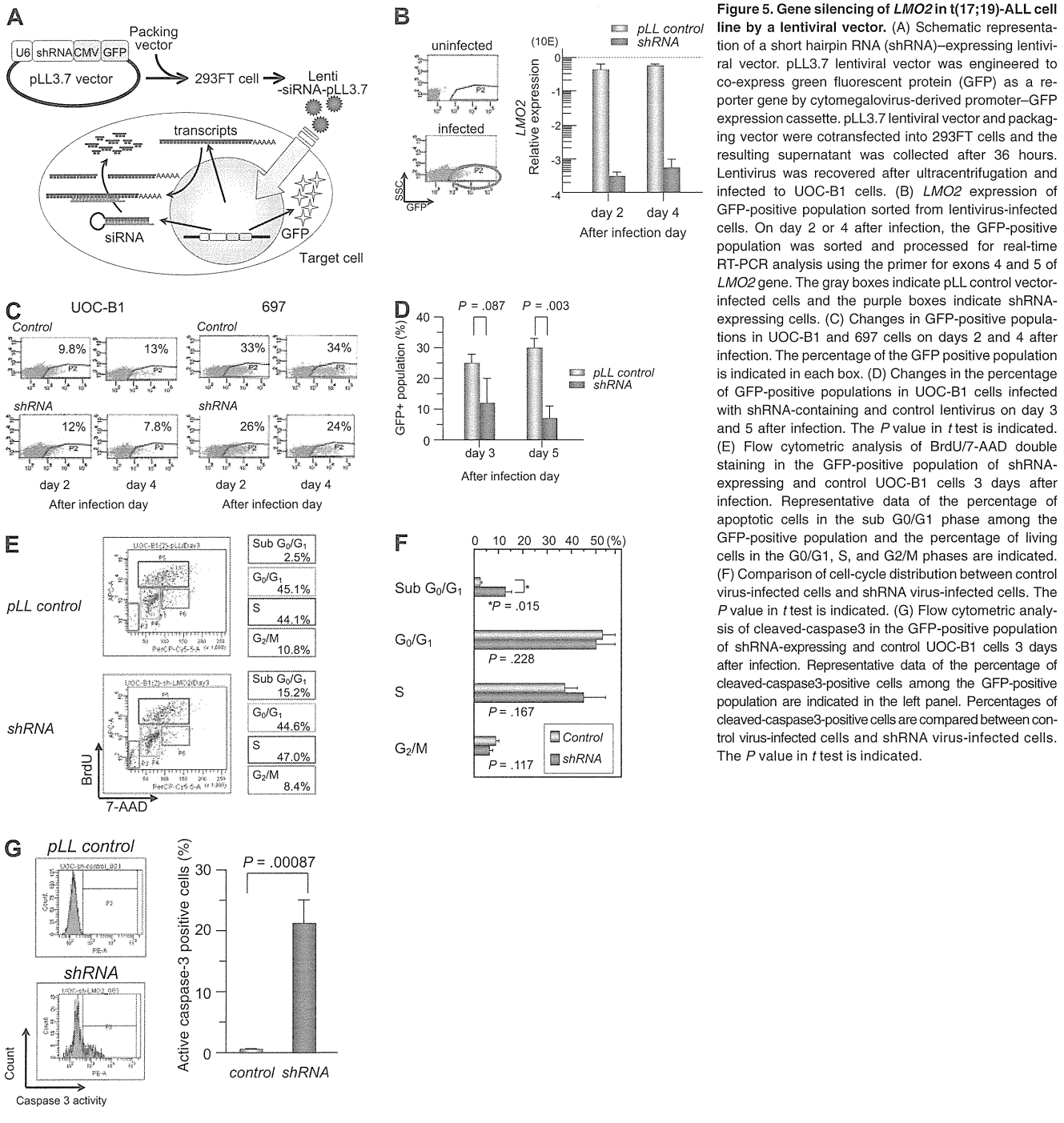

Figure 5. Gene silencing of *LMO2* in t(17;19)-ALL cell line by a lentiviral vector. (A) Schematic representation of a short hairpin RNA (shRNA)–expressing lentiviral vector. pLL3.7 lentiviral vector was engineered to co-express green fluorescent protein (GFP) as a reporter gene by cytomegalovirus-derived promoter–GFP expression cassette. pLL3.7 lentiviral vector and packaging vector were cotransfected into 293FT cells and the resulting supernatant was collected after 36 hours. Lentivirus was recovered after ultracentrifugation and infected to UOC-B1 cells. (B) *LMO2* expression of GFP-positive population sorted from lentivirus-infected cells. On day 2 or 4 after infection, the GFP-positive population was sorted and processed for real-time RT-PCR analysis using the primer for exons 4 and 5 of *LMO2* gene. The gray boxes indicate pLL control vector-infected cells and the purple boxes indicate shRNA-expressing cells. (C) Changes in GFP-positive populations in UOC-B1 and 697 cells on days 2 and 4 after infection. The percentage of the GFP positive population is indicated in each box. (D) Changes in the percentage of GFP-positive populations in UOC-B1 cells infected with shRNA-containing and control lentivirus on day 3 and 5 after infection. The *P* value in *t* test is indicated. (E) Flow cytometric analysis of BrdU/7-AAD double staining in the GFP-positive population of shRNA-expressing and control UOC-B1 cells 3 days after infection. Representative data of the percentage of apoptotic cells in the sub G0/G1 phase among the GFP-positive population and the percentage of living cells in the G0/G1, S, and G2/M phases are indicated. (F) Comparison of cell-cycle distribution between control virus-infected cells and shRNA virus-infected cells. The *P* value in *t* test is indicated. (G) Flow cytometric analysis of cleaved-caspase3 in the GFP-positive population of shRNA-expressing and control UOC-B1 cells 3 days after infection. Representative data of the percentage of cleaved-caspase3-positive cells among the GFP-positive population are indicated in the left panel. Percentages of cleaved-caspase3-positive cells are compared between control virus-infected cells and shRNA virus-infected cells. The *P* value in *t* test is indicated.

11p12-13 resulting in loss of negative regulatory sequences of the *LMO2* gene.[44] These 2 chromosomal abnormalities directly induce aberrant expression of the *LMO2* gene. Here we demonstrated a novel mechanism for aberrant expression of the *LMO2* gene as a downstream target of E2A-HLF fusion transcript derived from t(17;19) based on the following observations: all 4 t(17;19)-ALL cell lines studied and a patient's sample expressed a high level of *LMO2* gene transcript, and transfection of *E2A-HLF* into 697 cells induced gene expression of *LMO2* that was dependent on the transactivation and DNA-binding activities of E2A-HLF. E2A-HLF specifically bound to the PAR site in the distal promoter of the *LMO2* gene at least in vitro and enhanced promoter activity. Moreover, *LMO2* transcripts derived from both the proximal and distal promoters were expressed in t(17;19)-ALL cell lines. E2A-HLF rapidly induced *LMO2* gene expression originating from the distal promoter, and then induced *LMO2* gene expression derived from the proximal promoter, suggesting that E2A-HLF induces *LMO2* gene expression not only directly through the PAR site in the distal promoter but also indirectly through the proximal promoter.

It has been reported that LMO2 expression is down-regulated during T-cell development at the transition from immature CD4/CD8 double-negative thymocytes to more mature stages[16] and that enforced expression of *LMO2* in thymocytes blocks differentiation of CD4/CD8 double-negative thymocytes and induces T-cell malignancies.[17-20] In the present study, we confirmed that *LMO2* gene expression in both EBV-transformed normal B-cell lines and Burkitt B-cell lines was significantly lower than that in B-precursor ALL cell lines. In particular, LMO2 protein expression was almost

undetectable in these normal and leukemic B-cell lines. Moreover, the *LMO2* gene expression level was markedly down-regulated during the transition from CD19-negative to CD19-positive population in the cord blood $CD34^+$MNCs. These data are in agreement with the down-regulation of *LMO2* gene expression during the early phase in the normal progression of B-cell development.[19] Of note, gene silencing of *LMO2* by the introduction of shRNA using lentivirus vector induced specific cell death. Interestingly, a recent analysis by Natkunam et al[15] demonstrated that the majority of CD10-positive germinal center B cells coexpressed LMO2 while $CD79a^+$ plasma cells lacked LMO2 expression, suggesting the association of LMO2 down-regulation with normal B-cell development. These observations seem to be in agreement with the assumption that aberrant expression of LMO2 is involved in the maturation arrest of t(17;19)-ALL cells at the immature B-precursor stage. Taken together, LMO2 expression is down-regulated during the normal development of both T cells and B cells, and its aberrant expression promotes cell survival of immature lymphocytes, which subsequently contributes to leukemogenesis of both T-ALL and B-precursor ALL. In this context, it should be noted that approximately one-fourth of non-t(17;19) B-precursor ALL cell lines expressed LMO2 at an equivalent level to that in t(17;19)-ALL cell lines, suggesting that LMO2 might also play a role, at least in part, in the leukemogenesis of other types of B-precursor ALL. Finally, considering the dismal outcome of conventional chemotherapy for t(17;19)-ALL cases,[45] the development of new therapeutic modalities is urgently needed. Here we demonstrated that gene silencing of *LMO2* using shRNA specifically induced cell death of t(17;19)-ALL cells. Thus, there is a possibility that aberrantly expressed LMO2 in t(17;19)-ALL might become a possible target for therapy.

Authorship

Contribution: K.H. performed most of experiments and analyzed the data; T. Inukai designed the project, analyzed the data, and wrote the manuscript; J.K. and Y.F. performed shRNA analysis; T. Ikawa, H. Kawamoto, H. Kurosawa, A.T.L., and H.M. provided tools for analysis; S.H.O., B.G, N.K., Y.M., and H.O. performed gene expression analysis; K.A., X.Z., I.K., H.H., K.K., and K.G. performed analysis of cell line; T. Inaba wrote the manuscript; and K.S. supervised the project and wrote the manuscript.

Conflict-of-interest disclosure: The authors declare no competing financial interests.

Correspondence: Dr Takeshi Inukai, Department of Pediatrics, School of Medicine, University of Yamanashi, 1110 Shimokato, Chuo, Yamanashi 409-3898, Japan; e-mail: tinukai@yamanashi.ac.jp.

References

1. Rabbitts TH. Chromosomal translocations in human cancer. *Nature.* 1994;372(6502):143-149.
2. Look AT. Oncogenic transcription factors in the human acute leukemias. *Science.* 1997; 278(5340):1059-1064.
3. Boehm T, Foroni L, Kaneko Y, Perutz MF, Rabbitts TH. The rhombotin family of cysteine-rich LIM-domain oncogenes: distinct members are involved in T-cell translocations to human chromosomes 11p15 and 11p13. *Proc Natl Acad Sci U S A.* 1991;88(10):4367-4371.
4. Royer-Pokora B, Loos U, Ludwig WD. TTG-2, a new gene encoding a cysteine-rich protein with the LIM motif, is overexpressed in acute T-cell leukaemia with the t(11;14)(p13;q11). *Oncogene.* 1991;6(10):1887-1893.
5. Wadman I, Li J, Bash RO, et al. Specific in vivo association between the bHLH and LIM proteins implicated in human T cell leukemia. *EMBO J.* 1994;13(20):4831-4839.
6. Wadman IA, Osada H, Grutz GG, et al. The LIM-only protein Lmo2 is a bridging molecule assembling an erythroid, DNA-binding complex which includes the TAL1, E47, GATA-1 and Ldb1/NLI proteins. *EMBO J.* 1997;16(11):3145-3157.
7. Agulnick AD, Taira M, Breen JJ, Tanaka T, Dawid IB, Westphal H. Interactions of the LIM-domain-binding factor Ldb1 with LIM homeodomain proteins. *Nature.* 1996;384(6606):270-272.
8. Grütz GG, Bucher K, Lavenir I, Larson T, Larson R, Rabbitts TH. The oncogenic T cell LIM-protein Lmo2 forms part of a DNA-binding complex specifically in immature T cells. *EMBO J.* 1998; 17(16):4594-4605.
9. Warren AJ, Colledge WH, Carlton MB, Evans MJ, Smith AJ, Rabbitts TH. The oncogenic cysteine-rich LIM domain protein rbtn2 is essential for erythroid development. *Cell.* 1994;78(1):45-57.
10. Yamada Y, Warren AJ, Dobson C, Forster A, Pannell R, Rabbitts TH. The T cell leukemia LIM protein Lmo2 is necessary for adult mouse hematopoiesis. *Proc Natl Acad Sci U S A.* 1998;95(7): 3890-3895.
11. Yamada Y, Pannell R, Forster A, Rabbitts TH. The oncogenic LIM-only transcription factor Lmo2 regulates angiogenesis but not vasculogenesis in mice. *Proc Natl Acad Sci U S A.* 2000;97(1):320-324.
12. Akashi K, He X, Chen J, Iwasaki H, Niu C, Steenhard B, Zhang J, Haug J, Li L. Transcriptional accessibility for genes of multiple tissues and hematopoietic lineages is hierarchically controlled during early hematopoiesis. *Blood.* 2003; 101(2):383-389.
13. Alizadeh AA, Eisen MB, Davis RE, et al. Distinct types of diffuse large B-cell lymphoma identified by gene expression profiling. *Nature.* 2000; 403(6769):503-511.
14. Lossos IS, Czerwinski DK, Alizadeh AA, et al. Prediction of survival in diffuse large-B-cell lymphoma based on the expression of six genes. *N Engl J Med.* 2004;350(18):1828-1837.
15. Natkunam Y, Zhao S, Mason DY, et al. The oncoprotein LMO2 is expressed in normal germinal-center B cells and in human B-cell lymphomas. *Blood.* 2007;109(4):1636-1642.
16. McCormack MP, Forster A, Drynan L, Pannell R, Rabbitts TH. The LMO2 T-cell oncogene is activated via chromosomal translocations or retroviral insertion during gene therapy but has no mandatory role in normal T-cell development. *Mol Cell Biol.* 2003;23(24):9003-9013.
17. Fisch P, Boehm T, Lavenir I, et al. T-cell acute lymphoblastic lymphoma induced in transgenic mice by the RBTN1 and RBTN2 LIM-domain genes. *Oncogene.* 1992;7(12):2389-2397.
18. Larson RC, Fisch P, Larson TA, et al. T cell tumours of disparate phenotype in mice transgenic for Rbtn-2. *Oncogene.* 1994;9(12):3675-3681.
19. Larson RC, Osada H, Larson TA, Lavenir I, Rabbitts TH. The oncogenic LIM protein Rbtn2 causes thymic developmental aberrations that precede malignancy in transgenic mice. *Oncogene.* 1995;11(5):853-862.
20. Neale GA, Rehg JE, Goorha RM. Ectopic expression of rhombotin-2 causes selective expansion of CD4-CD8- lymphocytes in the thymus and T-cell tumors in transgenic mice. *Blood.* 1995;86(8): 3060-3071.
21. Hacein-Bey-Abina S, Von Kalle C, Schmidt M, et al. LMO2-associated clonal T cell proliferation in two patients after gene therapy for SCID-X1. *Science.* 2003;302(5644):415-419.
22. McCormack MP, Rabbitts TH. Activation of the T-cell oncogene LMO2 after gene therapy for X-linked severe combined immunodeficiency. *N Engl J Med.* 2004;350(9):913-922.
23. Royer-Pokora B, Rogers M, Zhu TH, Schneider S, Loos U, Bolitz U. The TTG-2/RBTN2 T cell oncogene encodes two alternative transcripts from two promoters: the distal promoter is removed by most 11p13 translocations in acute T cell leukaemia's (T-ALL). *Oncogene.* 1995;10(7):1353-1360.
24. Landry JR, Kinston S, Knezevic K, Donaldson IJ, Green AR, Gottgens B. Fli1, Elf1, and Ets1 regulate the proximal promoter of the LMO2 gene in endothelial cells. *Blood.* 2005;106(8):2680-2687.
25. Crable SC, Anderson KP. A PAR domain transcription factor is involved in the expression from a hematopoietic-specific promoter for the human LMO2 gene. *Blood.* 2003;101(12):4757-4764.
26. Inaba T, Roberts WM, Shapiro LH, et al. Fusion of the leucine zipper gene HLF to the E2A gene in human acute B-lineage leukemia. *Science.* 1992; 257(5069):531-534.
27. Hunger SP, Ohyashiki K, Toyama K, Cleary ML. Hlf, a novel hepatic bZIP protein, shows altered DNA-binding properties following fusion to E2A in t(17;19) acute lymphoblastic leukemia. *Genes Dev.* 1992;6(9):1608-1620.
28. Mueller CR, Maire P, Schibler U. DBP, a liver-enriched transcriptional activator, is expressed late in ontogeny and its tissue specificity is determined posttranscriptionally. *Cell.* 1990;61(2):279-291.
29. Drolet D, Scully K, Simmons D, et al. TEF, a transcription factor expressed specifically in the anterior pituitary during embryogenesis, defines a new class of leucine zipper proteins. *Genes Dev.* 1991;5(10):1739-1753.
30. Yoshihara T, Inaba T, Shapiro LH, Kato JY, Look AT. E2A-HLF-mediated cell transformation requires both the trans-activation domains of E2A and the leucine zipper dimerization domain of HLF. *Mol Cell Biol.* 1995;15(6):3247-3255.

31. Inukai T, Inaba T, Yoshihara T, Look AT. Cell transformation mediated by homodimeric E2A-HLF transcription factors. *Mol Cell Biol.* 1997;17(3):1417-1424.
32. Inaba T, Inukai T, Yoshihara T, et al. Reversal of apoptosis by the leukaemia-associated E2A-HLF chimaeric transcription factor. *Nature.* 1996;382(6591):541-544.
33. Inukai T, Inaba T, Ikushima S, Look AT. The AD1 and AD2 transactivation domains of E2A are essential for the antiapoptotic activity of the chimeric oncoprotein E2A-HLF. *Mol Cell Biol.* 1998;18(10):6035-6043.
34. Inukai T, Inaba T, Dang J, et al. TEF, an antiapoptotic bZIP transcription factor related to the oncogenic E2A-HLF chimera, inhibits cell growth by down-regulating expression of the common beta chain of cytokine receptors. *Blood.* 2005;105(11):4437-4444.
35. Smith KS, Rhee JW, Naumovski L, Cleary ML. Disrupted differentiation and oncogenic transformation of lymphoid progenitors in E2A-HLF transgenic mice. *Mol Cell Biol.* 1999;19(6):4443-4451.
36. Honda H, Inaba T, Suzuki T, et al. Expression of E2A-HLF chimeric protein induced T-cell apoptosis, B-cell maturation arrest, and development of acute lymphoblastic leukemia. *Blood.* 1999;93(9):2780-2790.
37. Inaba T, Shapiro LH, Funabiki T, et al. DNA-binding specificity and trans-activating potential of the leukemia-associated E2A-hepatic leukemia factor fusion protein. *Mol Cell Biol.* 1994;14(5):3403-3413.
38. Hunger SP, Brown R, Cleary ML. DNA-binding and transcriptional regulatory properties of hepatic leukemia factor (HLF) and the t(17;19) acute lymphoblastic leukemia chimera E2A-HLF. *Mol Cell Biol.* 1994;14(9):5986-5996.
39. Inukai T, Zhang X, Goto M, et al. Resistance of infant leukemia with MLL rearrangement to tumor necrosis factor-related apoptosis-inducing ligand: a possible mechanism for poor sensitivity to antitumor immunity. *Leukemia.* 2006;20(12):2119-2129.
40. Uno K, Inukai T, Kayagaki N, et al. TNF-related apoptosis-inducing ligand (TRAIL) frequently induces apoptosis in Philadelphia chromosome-positive leukemia cells. *Blood.* 2003;101(9):3658-3667.
41. Rubinson DA, Dillon CP, Kwiatkowski AV, et al. A lentivirus-based system to functionally silence genes in primary mammalian cells, stem cells and transgenic mice by RNA interference. *Nat Genet.* 2003;33(3):401-406.
42. Kikuchi J, Shimizu R, Wada T, et al. E2F-6 suppresses growth-associated apoptosis of human hematopoietic progenitor cells by counteracting proapoptotic activity of E2F-1. *Stem Cells.* 2007;25(10):2439-2447.
43. Garcia IS, Kaneko Y, Gonzalez-Sarmiento R, et al. A study of chromosome 11p13 translocations involving TCR beta and TCR delta in human T cell leukaemia. *Oncogene.* 1991;6(4):577-582.
44. Van Vlierberghe P, van Grotel M, Beverloo HB, et al. The cryptic chromosomal deletion del(11)(p12p13) as a new activation mechanism of LMO2 in pediatric T-cell acute lymphoblastic leukemia. *Blood.* 2006;108(10):3520-3529.
45. Inukai T, Hirose K, Inaba T, Kurosawa H, et al. Hypercalcemia in childhood acute lymphoblastic leukemia: frequent implication of parathyroid hormone-related peptide and E2A-HLF from translocation 17;19. *Leukemia.* 2007;21(2):288-296.

Extensive gene deletions in Japanese patients with Diamond-Blackfan anemia

Madoka Kuramitsu,[1] Aiko Sato-Otsubo,[2] Tomohiro Morio,[3] Masatoshi Takagi,[3] Tsutomu Toki,[4] Kiminori Terui,[4] RuNan Wang,[4] Hitoshi Kanno,[5] Shouichi Ohga,[6] Akira Ohara,[7] Seiji Kojima,[8] Toshiyuki Kitoh,[9] Kumiko Goi,[10] Kazuko Kudo,[11] Tadashi Matsubayashi,[12] Nobuo Mizue,[13] Michio Ozeki,[14] Atsuko Masumi,[1] Haruka Momose,[1] Kazuya Takizawa,[1] Takuo Mizukami,[1] Kazunari Yamaguchi,[1] Seishi Ogawa,[2] Etsuro Ito,[4] and Isao Hamaguchi[1]

[1]Department of Safety Research on Blood and Biological Products, National Institute of Infectious Diseases, Tokyo, Japan; [2]Cancer Genomics Project, Graduate School of Medicine, The University of Tokyo, Tokyo, Japan; [3]Department of Pediatrics and Developmental Biology, Graduate School of Medicine, Tokyo Medical and Dental University, Bunkyo-ku, Tokyo, Japan; [4]Department of Pediatrics, Hirosaki University Graduate School of Medicine, Hirosaki, Japan; [5]Department of Transfusion Medicine and Cell Processing, Tokyo Women's Medical University, Tokyo, Japan; [6]Department of Pediatrics, Graduate School of Medical Sciences, Kyushu University, Fukuoka, Japan; [7]First Department of Pediatrics, Toho University School of Medicine, Tokyo, Japan; [8]Department of Pediatrics, Nagoya University Graduate School of Medicine, Nagoya, Japan; [9]Department of Hematology/Oncology, Shiga Medical Center for Children, Shiga, Japan; [10]Department of Pediatrics, School of Medicine, University of Yamanashi, Yamanashi, Japan; [11]Division of Hematology and Oncology, Shizuoka Children's Hospital, Shizuoka, Japan; [12]Department of Pediatrics, Seirei Hamamatsu General Hospital, Shizuoka, Japan; [13]Department of Pediatrics, Kushiro City General Hospital, Hokkaido, Japan; and [14]Department of Pediatrics, Graduate School of Medicine, Gifu University, Gifu, Japan

Fifty percent of Diamond-Blackfan anemia (DBA) patients possess mutations in genes coding for ribosomal proteins (RPs). To identify new mutations, we investigated large deletions in the RP genes *RPL5*, *RPL11*, *RPL35A*, *RPS7*, *RPS10*, *RPS17*, *RPS19*, *RPS24*, and *RPS26*. We developed an easy method based on quantitative-PCR in which the threshold cycle correlates to gene copy number. Using this approach, we were able to diagnose 7 of 27 Japanese patients (25.9%) possessing mutations that were not detected by sequencing. Among these large deletions, similar results were obtained with 6 of 7 patients screened with a single nucleotide polymorphism array. We found an extensive intragenic deletion in *RPS19*, including exons 1-3. We also found 1 proband with an *RPL5* deletion, 1 patient with an *RPL35A* deletion, 3 with *RPS17* deletions, and 1 with an *RPS19* deletion. In particular, the large deletions in the *RPL5* and *RPS17* alleles are novel. All patients with a large deletion had a growth retardation phenotype. Our data suggest that large deletions in RP genes comprise a sizable fraction of DBA patients in Japan. In addition, our novel approach may become a useful tool for screening gene copy numbers of known DBA genes. (*Blood*. 2012;119(10): 2376-2384)

Introduction

Diamond-Blackfan anemia (DBA; MIN# 105650) is a rare congenital anemia that belongs to the inherited BM failure syndromes, generally presenting in the first year of life. Patients typically present with a decreased number of erythroid progenitors in their BM.[1] A main feature of the disease is red cell aplasia, but approximately half of patients show growth retardation and congenital malformations in the craniofacial, upper limb, cardiac, and urinary systems. Predisposition to cancer, in particular acute myeloid leukemia and osteogenic sarcoma, is also characteristic of the disease.[2]

Mutations in the *RPS19* gene were first reported in 25% of DBA patients by Draptchinskaia et al in 1999.[3] Since that initial finding, many genes that encode large (RPL) or small (RPS) ribosomal subunit proteins were found to be mutated in DBA patients, including *RPL5* (approximately 21%), *RPL11* (approximately 9.3%), *RPL35A* (3.5%), *RPS7* (1%), *RPS10* (6.4%), *RPS17* (1%), *RPS24* (2%), and *RPS26* (2.6%).[4-7] To date, approximately half of the DBA patients analyzed have had a mutation in one of these genes. Konno et al screened 49 Japanese patients and found that 30% (12 of 49) carried mutations.[8] In addition, our data showed that 22 of 68 DBA patients (32.4%) harbored a mutation in ribosomal protein (RP) genes (T.T., K.T., R.W., and E.I., unpublished observation, April 16, 2011). These abnormalities of RP genes cause defects in ribosomal RNA processing, formation of either the large or small ribosome subunit, and decreased levels of polysome formation,[4-6,9-12] which is thought to be one of the mechanisms for impairment of erythroid lineage differentiation.

Although sequence analyses of genes responsible for DBA are well established and have been used to identify new mutations, it is estimated that approximately half of the mutations remain to be determined. Because of the difficulty of investigating whole allele deletions, there have been few reports regarding allelic loss in DBA, and they have only been reported for *RPS19* and *RPL35A*.[3,6,13] However, a certain percentage of DBA patients are thought to have a large deletion in RP genes. Therefore, a detailed analysis of allelic loss mutations should be conducted to determine other RP genes that might be responsible for DBA.

In the present study, we investigated large deletions using our novel approach for gene copy number variation analysis based on quantitative-PCR and a single nucleotide polymorphism (SNP) array. We screened Japanese DBA patients and found 7 patients with a large deletion in an allele in *RPL5*, *RPL35A*, *RPS17*, or *RPS19*. Interestingly, all of these patients with a large deletion had a phenotype of growth retardation, including short stature and

Submitted July 24, 2011; accepted November 15, 2011. Prepublished online as *Blood* First Edition paper, January 18, 2012; DOI 10.1182/blood-2011-07-368662.

The online version of this article contains a data supplement.

The publication costs of this article were defrayed in part by page charge payment. Therefore, and solely to indicate this fact, this article is hereby marked "advertisement" in accordance with 18 USC section 1734.

Table 1. Primers used for synchronized quantitative-PCR (s-q-PCR) of RPL proteins

Gene	Primer name	Sequence	Primer name	Sequence	Size, bp
RPL5	L5-02F	CTCCCAAAGTGCTTGAGATTACAG	L5-02R	CACCTTTTCCTAACAAATTCCCAAT	132
	L5-05F	AGCCCTCCAACCTAGGTGACA	L5-05R	GAATTGGGATGGGCAAGAACT	102
	L5-17F	TGAACCCTTGCCCTAAAACATG	L5-17R	TCTTGGTCAGGCCCTGCTTA	105
	L5-19F	ATTGTGCAAACTCGATCACTAGCT	L5-19R	GTGTCTGAGGCTAACACATTTCCAT	103
	L5-21F	GTGCCACTCTCTTGGACAAACTG	L5-21R	CATAGGGCCAAAAGTCAAATAGAAG	102
	L5-28F	TCCACTTTAGGTAGGCGAAACC	L5-28R	TCAGATTTGGCATGTACCTTTCA	102
RPL11	L11-06F	GCACCCACATGGCTTAAAGG	L11-6R	CAACCAACCCATAGGCCAAA	102
	L11-20F	GAGCCCCCTTTCTCAGATGATA	L11-20R	CATGAACTTGGGCTCTGAATCC	109
	L11-22F	TATGTGCAGATAAGAGGGCAGTCT	L11-22R	ATACAGATAAGGAAACTGAGGCAGATT	98
RPL19	L19-02F	TGGCCTCTCATAAAGGAAATCTCT	L19-02R	GGAATGCAGGCAAGTTACTCTGTT	103
	L19-08F	TTTGAAGGCAAGAAATAAGTTCCA	L19-08R	AGCACATCACAGAGTCCAAATAGG	107
	L19-16F	GGTTAGTTGAAGCAGGAGCCTTT	L19-16R	TGCTAGGGAGACAGAAGCACATC	102
	L19-19F	GGACCAGTAGTTGTGACATCAGTTAAG	L19-19R	CCCATTTGTAACCCCCACTTG	106
RPL26	L26-03F	TCCAAAGAGCTGAGACAGAAGTACA	L26-03R	TCCATCAAGACAACGAGAACAAGT	102
	L26-16F	TTTGAGAATGCTTGAGAGAAGGAA	L26-16R	TTCCAGCACATGTAAAATCAAGGA	102
	L26-18F	ATGTTTTAATAAGCCCTCCAGTTGA	L26-18R	GAGAACAGCAAGTTGAAAGGTTCA	102
	L26-20F	GGGCTTTGCTTGATCACTCTAGA	L26-20R	AGGGAGCCCGAAAACATTTAC	104
RPL35A	L35A-01F	TGTGGCTTCTATTTTGCGTCAT	L35A-01R	GGAATTACCTCCTTTATTGCTTACAAG	121
	L35A-07F	TTTCCGTTCTGTCTATTGCTGTGT	L35A-07R	GAACCCTGAGTGGAGGATGTTC	113
	L35A-17F	GCCCACAACCTCCAGAGAATC	L35A-17R	GGATCACTTGAGGCCAGGAAT	104
	L35A-18F	TTAGGTGGGCTTTTCAGTCTCAA	L35A-18R	ATCTCCTGATTCCCCAACTTTGT	102
RPL36	L36-02F	CCGCTCTACAAGTGAAGAAATTCTG	L36-02R	CTCCCTCTGCCTGTGAAATGA	102
	L36-04F	TGCGTCCTGCCAGTGTTG	L36-04R	GGGTAGCTGTGAGAACCAAGGT	105
	L36-17F	CCCCTTGAAAGGACAGCAGTT	L36-17R	TTGGACACCAGGCACAGACTT	114

Table 2. Primers used for s-q-PCR of RPS proteins

Gene	Primer name	Sequence	Primer name	Sequence	Size, bps
RPS7	S7-11F	GCGCTGCCAGATAGGAAATC	S7-11R	TTAGGGAGCTGCCTTACATATGG	102
	S7-12F	ACTGGCAGTTCTGTGATGCTAAGT	S7-12R	ACTCTTGCTCATCTCCAAAACCA	102
	S7-16F	GTGTCTGTGCCAGAAAGCTTGA	S7-16R	GAACCATGCAAAAGTGCCAATAT	112
RPS10	S10-03F	CTACGGTTTTGTGTGGGTCACTT	S10-03R	CATCTGCAAGAAGGAGACGATTG	102
	S10-15F	GTTGGCCTGGAGTCGTGATTT	S10-15R	ATTCCAAGTGCACCATTTCCTT	101
	S10-17F	AATGGTGTTTAGGCCAACGTTAC	S10-17R	TTTGAACAGTGGTTTTTGTGCAT	100
RPS14	S14-03F	GAATTCCAAACCCTTCTGCAAA	S14-03R	TTGCTTCATTTACTCCTCAAGACATT	104
	S14-05F	ACAACCAGCCCTCTACCTCTTTT	S14-05R	GGAAGACGCCGGCATTATT	102
	S14-06F	CGCCTCTACCTCGCCAAAC	S14-06R	GGGATCGGTGCTATTGTTATTCC	102
	S14-09F	GCCATCATGCCGAAACATACT	S14-09R	AACGCGCCACAGGAGAGA	102
	S14-13F	ATCAGGTGGAGCACAGGAAAAC	S14-13R	GCGAGGGAGCTGCTTGATT	111
	S14-15F	AGAAGTTTTAGTGAGGCAGAAATGAGA	S14-15R	TCCCCTGGCTATTAAATGAAACC	102
	S14-19F	GATGAATTGTCCTTTCCTCCATTC	S14-19R	TAGGCGGAAACCAAAAATGCT	102
RPS15	S15-11F	CTCAGCTAATAAAGGCGCACATG	S15-11R	CCTCACACCACGAACCTGAAG	108
	S15-15F	GGTTGGAGAACATGGTGAGAACTA	S15-15R	CACATCCCTGGGCCACTCT	108
RPS17	S17-03F	ACTGCTGTCGTGGCTCGATT	S17-03R	GATGACCTGTTCTTCTGGCCTTA	121
	S17-05F	GAAAACAGATACAAATGGCATGGT	S17-05R	TGCCTCCCACTTTTCCAGAGT	114
	S17-12F	CTATGTGTAGGAGGTCCCAGGATAG	S17-12R	CCACCTGGTACTGAGCACATGT	102
	S17-16F	TAGCGGAAGTTGTGTGCATTG	S17-16R	CAAGAACAGAAGCAGCCAAGAG	102
	S17-18F	TGGCTGAATCTGCCTGCTT	S17-18R	GCCTTGTATGTACCTGGAAATGG	103
	S17-20F	GGGCCCTTCACAAATGTTGA	S17-20R	GCAAAACTCTGTCCCTTTGAGAA	101
RPS19	S19-24F	CCATCCCAAGAATGCACACA	S19-24R	CGCCGTAGCTGGTACTCATG	120
	S19-28F	GACACACCTGTTGAGTCCTCAGAGT	S19-28R	GCTTCTATTAACTGGAGCACACATCT	114
	S19-36F	CTCTTGAGGGTGGTCTGGAAAT	S19-36R	GTCTTTGCGGGTTCTTCCTCTAC	102
	S19-40F	GGAACGGTGTCAGGATTCAAG	S19-40R	AGCGGCTGTACACCAGAAATG	101
	S19-44F	CTGAGGTTGAGTGTCCCATTTCT	S19-44R	GCACCGGGCCTCTGTTATC	104
	S19-57F	CAGGGACACAGTGCTGAGAAACT	S19-57R	TGAGATGTCCCATTTTCACTATTGTT	101
	S19-58F	CATGATGTTAGCTCCGTTGCATA	S19-58R	ATTTTGGGAAGAGTGAAGCTTAGGT	102
	S19-62F	GCAACAGAGCGAGACTCCATTT	S19-62R	AGCACTTTTCGGCACTTACTTCA	102
	S19-65F	ACATTTCCCAGAGCTGACATGA	S19-65R	TCGGGACACCTAGACCTTGCT	102
RPS24	S24-17F	CGACCACGTCTGGCTTAGAGT	S24-17R	CCTTCATGCCCAACCAAGTC	101
	S24-20F	ACAAGTAAGCATCATCACCTCGAA	S24-20R	TTTCCCTCACAGCTATCGTATGG	105
	S24-32F	GGGAAATGCTGTGTCCACATACT	S24-32R	CTGGTTTCATGGCTCCAGAGA	105
RPS26	S26-03F	CGCAGCAGTCAGGGACATTT	S26-03R	AAGTTGGGCGAAGGCTTTAAG	104
	S26-05F	ATGGAGGCCGTCTAGTTTGGT	S26-05R	TGCCTACCCTGAACCTTGCT	102
RPS27A	S27A-09F	GCTGGAGTGCATTCGCTTGT	S27A-09R	CACGCCTGTAATCCCCACTAA	102
	S27A-12F	CAGGCTTGGTGTGCTGTGACT	S27A-12R	ACGTCCATCTTCCAGCTGCTT	103
	S27A-18F	GGGTTTTTCCTGTTTGGTATTTGA	S27A-18R	AAAGGCCAGCTTTGCAAGTG	111
	S27A-22F	TTACCATATTGCCAGTCTTTCCATT	S27A-22R	TTCATATGCATTTGCACAAACTGT	106